



5-2004

Finite Element Nonlinear Dynamic Response Analysis of the Human Knee Joint

T. Wayne Pfeiler
University of Tennessee, Knoxville

Follow this and additional works at: https://trace.tennessee.edu/utk_gradthes



Part of the [Engineering Science and Materials Commons](#)

Recommended Citation

Pfeiler, T. Wayne, "Finite Element Nonlinear Dynamic Response Analysis of the Human Knee Joint. " Master's Thesis, University of Tennessee, 2004.
https://trace.tennessee.edu/utk_gradthes/4804

This Thesis is brought to you for free and open access by the Graduate School at TRACE: Tennessee Research and Creative Exchange. It has been accepted for inclusion in Masters Theses by an authorized administrator of TRACE: Tennessee Research and Creative Exchange. For more information, please contact trace@utk.edu.

To the Graduate Council:

I am submitting herewith a thesis written by T. Wayne Pfeiler entitled "Finite Element Nonlinear Dynamic Response Analysis of the Human Knee Joint." I have examined the final electronic copy of this thesis for form and content and recommend that it be accepted in partial fulfillment of the requirements for the degree of Master of Science, with a major in Engineering Science.

Mehran Kasra, Major Professor

We have read this thesis and recommend its acceptance:

Chris Pionke, Jack Wasserman

Accepted for the Council:


Carolyn R. Hodges

Vice Provost and Dean of the Graduate School


(Original signatures are on file with official student records.)


To the Graduate Council:

I am submitting herewith a thesis written by T. Wayne Pfeiler entitled "Finite Element Nonlinear Dynamic Response Analysis of the Human Knee Joint." I have examined the final paper copy of this thesis for form and content and recommend that it be accepted in partial fulfillment of the requirements for the degree of Master of Science, with a major in Engineering Science.

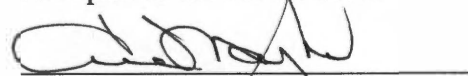

Mehran Kasra, Major Professor

We have read this thesis and
recommend its acceptance:


Chris Pionke


Jack Wasserman

Acceptance for the Council:


Vice Chancellor and Dean of
Graduate Studies

***FINITE ELEMENT NONLINEAR DYNAMIC
RESPONSE ANALYSIS OF THE
HUMAN KNEE JOINT***

A Thesis Presented for the
Master of Science Degree
The University of Tennessee, Knoxville

T. Wayne Pfeiler
May 2004

Thesis
2004
.P44

Dedication

This thesis is dedicated to my fiancée, Erika, whose tremendous work ethic has somehow managed to rub off on me, and my family who have supported me and encouraged me to realize my potential. I thank my sister, Lara, who greatly influenced my decision to study Biomedical Engineering. Growing up with Lara taught me that people who begin with great disadvantages could still achieve so much and impart much joy onto the lives of others.

Acknowledgements

I would like to thank all those who have assisted me in completing the Master of Science in Engineering Science, Biomedical concentration. I thank Dr. Mehran Kasra for his guidance and insight into using finite element software and for encouraging me to take on this thesis. I thank Shirazi-adl in Montreal for laying the groundwork that I have been able to build upon, and lending a helpful hand when we ran into troubles. I thank Dr. Yu for introducing me to the finite element method so that I might make use of it on my own. Lastly, I thank all my friends who have helped make my journey very enjoyable and much more memorable.

Abstract

Objective. To develop a detailed non-linear 3-D dynamic finite element model of the knee joint and perform preliminary analysis simulating different loading conditions to confirm reasonable function of the model.

Design. Using ANSYS, a finite element model of the human knee was created and tested.

Background. Finite element models of the knee have been developed in previous studies. However, no study has generated a detailed tissue level model, or performed dynamic testing on a model.

Methods. Initial cartilage and ligament geometry was received from a previous study. A finite element mesh including bone was created. The model was constrained to simulate different experimental testing conditions by rigidly fixing the distal tibia and limiting the motion of the proximal femur. Free vibration and steady state analyses of the model were performed simulating experiments.

Results. A detailed, highly nonlinear finite element model of the human knee was created in three dimensions. Axial compressive load and two constraint conditions were applied. Solution was performed to the point of easy convergence. The model was also examined through dynamic analysis to find the mode shapes. The model performed well under this initial analysis.

Conclusion. The model was developed and tested successfully. The model needs further refinement and verification with experimental data to follow. The preliminary analysis of the model indicated that constraint conditions could significantly affect the magnitude and distribution of stresses within the different components of the knee joint. Mode shapes are also varied at different constraint conditions. The model is applicable to predict the vulnerable parts of the knee joint at different clinical situations as well as occupational conditions.

Table of Contents

<i>Chapter</i>	<i>Page</i>
1. Introduction	1
Background	1
Previous Studies	3
Knee Anatomy	4
Objective	6
2. Methods and Materials	7
Initial Geometry	7
Mesh Generation	7
Contact Problem	10
Material Properties	11
Boundary Conditions	11
Nonlinear Analysis Parameters	14
Modal Analysis Parameters	14
3. Results	17
Deformation	17
Stress Distribution	19
Modal Analysis	21
4. Discussion	23
Clinical Application of the Model	23
Nonlinear Analysis	24
Deformation in Static Loading	25
Modal Analysis	25
Future Work	26
List of References	27
Appendix	33
Vita	65

List of Tables

<i>Table</i>		<i>Page</i>
1.	Material Properties Summary	12
2.	Density of Materials	15
3.	Frequencies and Mode Shapes	22

List of Figures

<i>Figure</i>	<i>Page</i>
1. Anterior Knee in Flexion and Extension	5
2. Patellofemoral Articular Cartilage	8
3. Tibial Articular Cartilage	8
4. Boundary Conditions Applied to Constrained Model	13
5. Boundary Conditions Applied to Coupled Model	13
6. Axial Femoral Displacement vs. Total Applied Load	18
7. Displacement of Entire Constrained Model	18
8. Stress Distribution in Entire Constrained Model	20
9. Stress Distribution in Entire Coupled Model	20
10. Mode 1 of Constrained Model	22
A1. Meniscus Body	35
A2. Fiber Reinforcement of Meniscus	35
A3. Ligaments	36
A4. Original Sawbones Model of Knee	36
A5. Subchondral Bone	37
A6. Section Markings on Sawbones	37
A7. Applying Magnet Wire to Sawbones	38
A8. Traced Outline of Magnet Wire	38
A9. Profiles of Section Geometry	39
A10. Cortical Bone	39
A11. Trabecular Bone	40
A12. Patella	40
A13. Contact Surfaces	41
A14. Completed Model, Posterior View	41
A15. Completed Model, Anterior View	42
A16. Displacement of Entire Coupled Model	42
A17. Displacement of Constrained Model Tibia	43
A18. Displacement of Coupled Model Tibia	43
A19. Displacement of Constrained Model Femur	44
A20. Displacement of Coupled Model Femur	44
A21. Deformation of Constrained Model Meniscus	45
A22. Deformation of Coupled Model Meniscus	45
A23. Stress Distribution in Constrained Model Femoral Cartilage	46
A24. Stress Distribution in Coupled Model Femoral Cartilage	46
A25. Stress Distribution in Constrained Model Tibial Cartilage	47
A26. Stress Distribution in Coupled Model Tibial Cartilage	47
A27. Stress Distribution in Constrained Model Meniscus	48
A28. Stress Distribution in Coupled Model Meniscus	48

Figure	Page
A29. Stress Distribution in Constrained Model Lateral Meniscus	49
A30. Stress Distribution in Coupled Model Lateral Meniscus	49
A31. Stress Distribution in Constrained Model Medial Meniscus	50
A32. Stress Distribution in Coupled Model Medial Meniscus	50
A33. Stress Distribution in Constrained Model Femur	51
A34. Stress Distribution in Coupled Model Femur	51
A35. Stress Distribution in Constrained Model Tibia	52
A36. Stress Distribution in Coupled Model Tibia	52
A37. Stress Distribution in Constrained Model Femoral Subchondral Bone	53
A38. Stress Distribution in Coupled Model Femoral Subchondral Bone	53
A39. Stress Distribution in Constrained Model Tibial Subchondral Bone	54
A40. Stress Distribution in Coupled Model Tibial Subchondral Bone	54
A41. Stress Distribution in Constrained Model Cortical Bone	55
A42. Stress Distribution in Coupled Model Cortical Bone	55
A43. Stress Distribution in Constrained Model Femoral Trabecular Bone	56
A44. Stress Distribution in Coupled Model Femoral Trabecular Bone	56
A45. Stress Distribution in Constrained Model Tibial Trabecular Bone	57
A46. Stress Distribution in Coupled Model Femoral Trabecular Bone	57
A47. Mode 2 of Constrained Model	58
A48. Mode 3 of Constrained Model	58
A49. Mode 4 of Constrained Model	59
A50. Mode 5 of Constrained Model	59
A51. Mode 6 of Constrained Model	60
A52. Mode 1 of Coupled Model	60
A53. Mode 2 of Coupled Model	61
A54. Mode 3 of Coupled Model	61
A55. Mode 4 of Coupled Model	62
A56. Mode 5 of Coupled Model	62
A57. Mode 6 of Coupled Model	63

Chapter 1: Introduction

Background

Mechanical factors play an important role in the cause of knee injuries and diseases such as osteoarthritis (OA). While performing daily activities such as walking, running, and climbing as well as during occupational and sport activities, the joint is exposed to vibrations and multiple impacts. There is some evidence that the cumulative effect of these impact forces may be harmful. For instance, researchers showed that repeated impulse loadings could produce degenerative changes in cartilage [Radin et al. 1973]. There is also a high risk of osteoarthritis in occupations involving repeated squatting and lifting tasks [Holibkova et al., 1989; Cooper, 1995]. Premature and posttraumatic osteoarthritis is common in elite athletes participating in sport activities involving multiple impacts on the knee joint such as soccer, cross-country skiing, ice hockey [Roos, 1998; Sandmark, 1996] as well as heavy weight-bearing such as weight lifters [Spector et al., 1996]. Even teenagers in high school sports are very susceptible to traumatic knee injury; with 60.3% of all United States school sports injuries requiring surgery involving the knee [Powell JW, Barber-Foss KD, 1999]. According to an individual's age, fitness, and weight, these activities may cause the joint load, stiffness, and damping to reach critical limits initiating or accelerating different knee disorders.

The knee joint is a complex nonlinear dynamic system acting as the main shock absorber of the body. Its shock absorbing property depends on the material behaviour of its constituents such as meniscus, cartilage, bones, etc. The knee joint dynamic behaviour is the main determinant of how ground impact forces are transmitted to the other upper load-bearing joints such as hip and spine. A reduced dynamic performance at the knee joint level not only has a deteriorating affect on different constituents like bone, cartilage, etc. of the knee joint itself but may also adversely affect hip joint and spine, increasing the risk of osteoarthritis and low-back pain [Wolfe et al., 1996].

The prevalence of knee OA increases with age throughout the elderly years [Felson et al., 1987]. Elderly persons at high risk of developing radiographic knee OA include obese persons and those who are physically active. There is also an increase in rate of OA following meniscectomy in young population [Neyret et al., 1994] and damage to the ACL. An increase in weight correlated directly with the risk of developing OA [Felson et al., 1997].

Musculoskeletal disorders, of which OA is the most common, cause significant economic, social, and psychological costs. Costs of illness have risen over recent decades accounting for up to 1-2.5% of the gross national product for those countries studied so far, including the USA, Canada, UK, France and Australia [March and Bachmeier, 1997]. Statistics show that over two million cases of knee injury occur in the United States each year. Inadequate understanding of the knee joint dynamic behavior results in poor preventive measures and management of these injuries. This will further increase the number of population suffering from knee osteoarthritis [Cooper, 1995; Roos, 1998; Spector et al., 1996] and the consequent low back pain [Wolfe et al., 1996]. Osteoarthritis is the most common form of arthritis targeting elderly as well as active age groups in the population. It can result in severe pain and disability and is becoming one of the great healthcare challenges of the future [Felson, 1996; Dieppe, 1993]. About 5% of the United States population is affected with hip or knee osteoarthritis. Because of the frequency, associated pain, and disability of this disease, osteoarthritis accounts for much of the disability in lower extremities. More than 70% of total hip and knee replacements are performed for osteoarthritis [Felson, 1996]. Osteoarthritis is one of the most important diseases as it frequently affects the active age group of the population and is the source of considerable loss of working hours and of disability [Cooper, 1995; Roos, 1998; Spector et al., 1996]. Because osteoarthritis is so common, identification of mechanical factors that increase osteoarthritis risk could prevent substantial pain and disability in the elderly as well as active age group and the use of costly health care services.

Overweight people are at higher risk of developing knee osteoarthritis. Furthermore, being overweight is considered as a risk factor in accelerating disease progression in knee OA. The health-related economic cost of obesity to U.S. business in 1994 was estimated to total \$12.7 billion. Osteoarthritis of the knee shares a substantial amount of this cost [Thompson et al., 1998]. Unfortunately, studies of metabolic factors linked to obesity have not provided an explanation for these findings [Felson and Chaisson, 1997]. In this case, the role of mechanical factors seems to be very important. Therefore, investigating the role of upper body mass and weight applied on the knee joint and its dynamic response may help develop a better understanding of the knee. A detailed nonlinear dynamic finite element model is ideally suited for this task, since it allows for investigation of the knee under varied circumstances. Creation of such a finite element model would also allow for many more future studies on knee pathology and degenerative effects leading to OA and other diseases.

Previous Studies

Computational models of the knee have been developed over the past several decades. However, these models leave much to be desired, since they often over-simplify the geometry and material properties of the knee. Several two dimensional models have been created [Gill HS, et al., 1996]. These may have been successful but limited to describing only the particular geometry they modeled. Three-dimensional analytical studies have become more common in recent years, and typically model the tibiofemoral joint [Abdel-Rahman, et al., 1993; Blankevoort L, et al, 1991; Wisman J, et al., 1980]. Some studies have also modeled the patellofemoral joint [Hirokawa S, 1991; van Eijden TMGJ, et al., 1986]. These studies typically model only surfaces and neglect the effect of ligaments and collagen fibers in meniscus. No study has yet created a tissue-level detailed 3D nonlinear dynamic model of the knee, as this study intends. Such a model would allow a more detailed analysis, such a vibration modal analysis.

Knee Anatomy

To understand the behavior of the knee, it is important to have a basic knowledge of its anatomy. Although the knee is the largest and the most complex joint in the human body, it may be better understood by considering its components. The knee [Figure 1] consists of bones, cartilage, meniscus, ligaments, and tendons. The weight-bearing bones involved are the femur and tibia. The third bone, the patella, serves as a gliding connection against the femur for the quadriceps tendons and patellar ligament in order to allow leg extension. The tibia and femur consist of different types of bone, layered in order to provide an optimal combination of strength and weight. The surface of these bones consists of cortical bone, the hardest, strongest, most dense type of bone in the body. Cortical bone serves as an outside shell around the less dense trabecular bone on all but the articular surfaces. The trabecular bone makes up the internal body of the bone. Although less dense, it also supports loading. At the articular surfaces of the distal femur and proximal tibia are layers of cartilage called condyles. These cartilage sheaths serve as low-friction bearing surface to allow smooth sliding and articulation of the joint in the healthy knee. Between the cartilage and trabecular bone is a layer of subchondral bone. This bone serves as a connection between the trabecular bone and the cartilage. It has strength and density properties between cortical and trabecular bone. Between the articular surfaces of the femur and tibia are medial and lateral crescent-shaped pads of fibrocartilage, called meniscus. These menisci can be considered as fiber-reinforced composites and serve as shock absorbers for impact of the leg. The tips, or horns, of the crescents insert to the center of the proximal tibia. Ligaments are string-like bundles of collagen fibers connecting the tibia and femur in order to provide stability and constrain motion of the knee. These ligaments are nonlinear in stress-strain characteristics. Tendons are the attachments of muscle to ligament and bone.

The normal knee allows for flexion and extension of the lower leg by bending at the tibiofemoral connection. As the knee joint flexes, the proximal tibia slides around the periphery of the femoral condyle to the posterior. Walking causes the joint to extend and

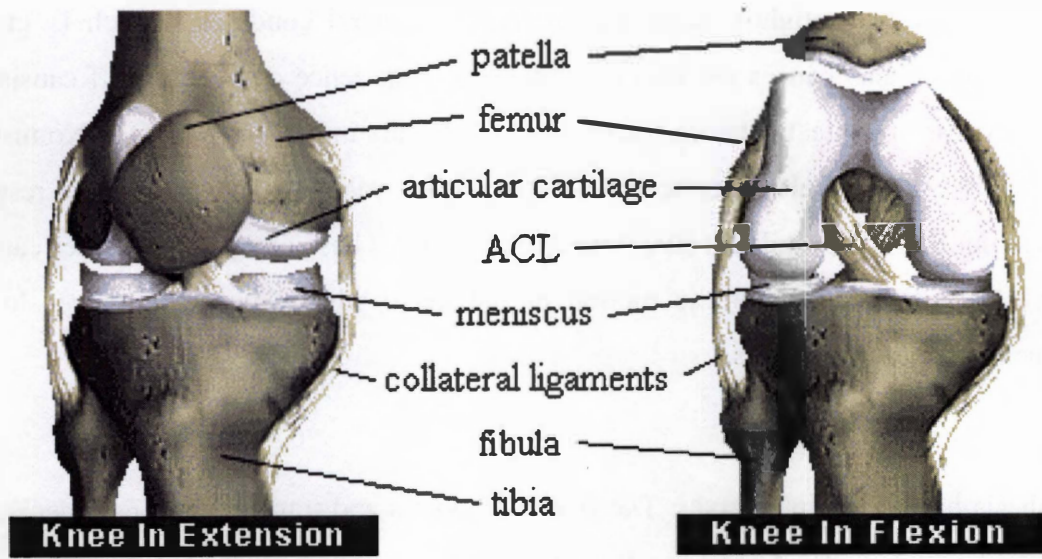


Figure 1: Anterior Knee in Flexion and Extension
(Tibia fixed at bottom in both views)

flex in a similar, but more complicated manner. The medial condyles of the tibia and femur typically bear slightly more weight than the lateral condyles [Kirsch L, et al., 1998]. Walking also causes the lateral condyles to experience a slight lift off causing a temporary loss of contact between the surfaces, especially in persons with OA [Komistek, et al., 1998]. The tibia also experiences a slight varus - valgus axial rotation with respect to the femur during normal gait [Freeman MAR, 2001]. These many complexities caused much early confusion about the motion of the knee, which appears to have slowly become clearer to researchers.

Objective

This thesis has several objectives. The first is to obtain and transfer cartilage, meniscus, and ligament geometry of the knee from the previous work of Shirazi-Adl in Montreal [Bendjaballah MZ et al., 1995] into an ANSYS¹-compatible batch file for use in finite element simulation. Then bone (cortical, trabecular, and subchondral) must be added to expand the geometry into a more complete model of the knee. The batch file must be written to solve for nonlinear dynamic analysis. Finally, the function of the model is checked by simple nonlinear static and modal analysis. Modal analysis is conducted at different constraint conditions for the benefit of an associated future experimental study of the knee, in order to estimate the knee joint resonant frequencies at different constraint conditions of interest and help develop experimental procedure.

¹ Version 8.0 ANSYS University – Intermediate. ANSYS, Inc. Canonsburg, PA

Chapter 2: Methods and Materials

Initial Geometry

The geometry data of articular surfaces and meniscus was first obtained from A Shirazi-Adl at *Ecole Polytechnique*, Montreal, Quebec, Canada [Bendjaballah MZ et al., 1995]. This data was gathered by applying computerized tomography (CT) to a fresh frozen cadaveric right knee joint from a 27 year-old woman. The joint was found to be radiologically and visually normal. The CT image data was taken in 1 mm thick sections on the sagittal plane. An in-house image processing program was used in Montreal to generate a three dimensional (3D) triangular solid mesh of the bone structure. Soft tissue geometry was obtained by a numerically controlled direct digitization machine, due to the inherent problem of soft tissue visibility on CT scan images. Next, the 3D Cartesian data was smoothed, patched, and gridded into a reconstructed form suitable for finite element modeling. Then a preliminary mesh was generated for the articular cartilage surfaces [Figures 2, 3]. Nonlinear data was added for fibrocartilage [Figures A1, A2] and ligaments [Figure A3].

Mesh Generation

We further developed the model by adding the geometries of femur and tibia bones to the contact geometry. In order to add the geometry of the bone extending beyond the cartilage surfaces provided, many calculations and measurements were made. All measurements were made on a Sawbones² knee model of the adult human knee [Figure A4]. This model included tibia and femur with cords approximating ligament connections. We had previous experience using such models of bone and were confident with the geometrical accuracy. The cords simulating ligaments were severed in order to allow better visualization and measurement of the condyles. All node and element creation was conducted first in the ANSYS GUI and then transferred to the batch file.

² Item # 1152, Pacific Research Laboratories. Vashon, Washington.

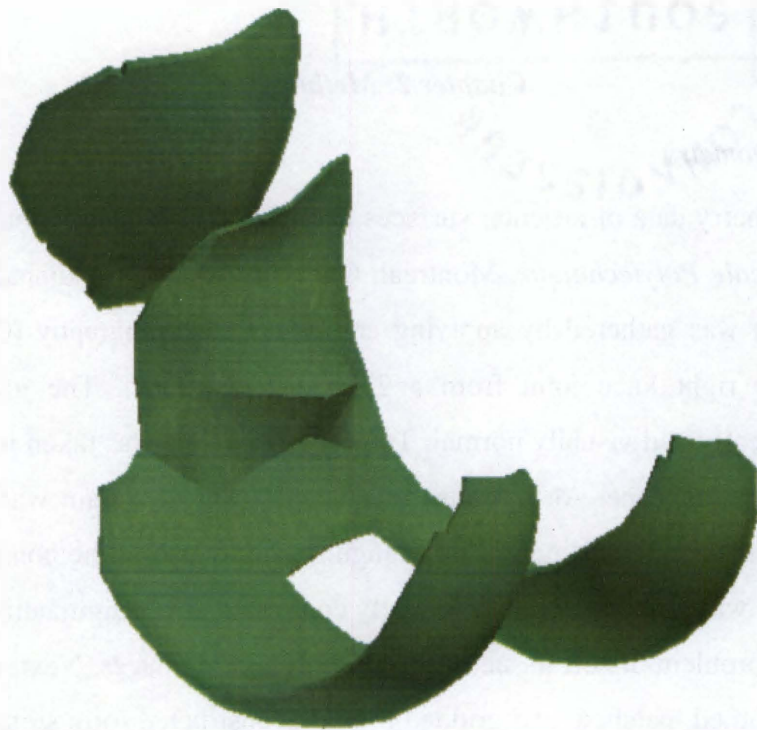


Figure 2: Patellofemoral Articular Cartilage

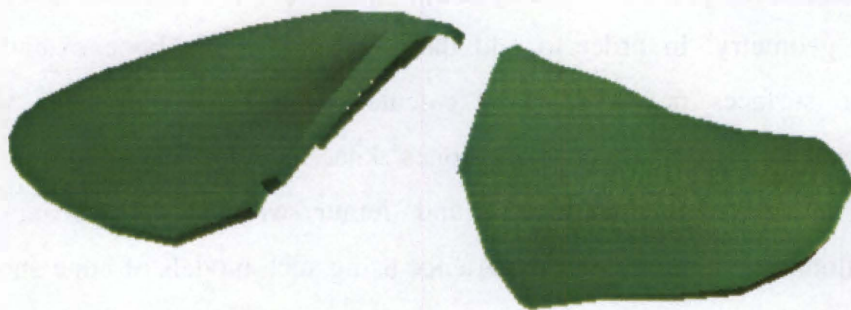


Figure 3: Tibial Articular Cartilage

To approximate the subchondral bone, a line extension algorithm was created to generate new nodes a chosen distance, ds , from existing nodal coordinates. This was applied to the femoral cartilage layer and elements were created to model the subchondral bone [Figure A5]. The equations used are as follows:

$$ds^2 = \Delta x^2 + \Delta y^2 + \Delta z^2$$

$$\beta = \Delta y / \Delta x$$

$$\gamma = \Delta z / \Delta x$$

$$\Delta x = \sqrt{\frac{ds^2}{1 + \beta^2 + \gamma^2}}$$

An attempt was made to use a coordinate measuring machine to gather data points for use in creating the cortical bone geometry of the femur. Unfortunately, this proved to be a very time intensive procedure, due to the age of available equipment, and was discarded. A faster method to collect geometric data was employed instead, as suggested by M Kasra. Transverse, or axial, sections were selected and marked on the sawbones model [Figure A6]. The increment of these sections was chosen to match the spacing of nodes in the existing element mesh. This geometry was recorded by applying a fine magnet wire to the surface of each section [Figure A7] and then tracing the wire outline onto paper [Figure A8]. The paper outlines were excised [Figure A9], scaled, oriented to the existing knee, and affixed to the computer monitor. Then a work plane was selected in the ANSYS graphical user interface (GUI) to match the section and nodes were added along the periphery of the paper outline. This allowed creation of the peripheral cortical bone geometry of the femur and tibia [Figure A10]. Internal nodes were created to generate the element layer of cortical bone. The thickness of this layer was chosen by referencing medical texts [Gray's Anatomy, 1995].

Nodes for trabecular bone [Figure A11] were created on each transverse layer of cortical bone. These nodes were first matched to existing geometry of the subchondral bone on

the distal femur, but later adjusted to a simplified grid pattern. This adjustment proved difficult in practice, and involved many 4-node tetrahedron elements. Elements were manually created for the prior layers of trabecular bone, and along the periphery of all layers. The internal elements of the simplified grid layers allowed for automatic element generation in ANSYS.

The tibia mesh was produced in a similar fashion to the femur, except for generation of the intercondylar space. This was produced by approximating a straight line between the existing articular surfaces. The finite element mesh generation primarily consisted of 8-node (solid45) brick elements, however 6-node wedge elements and 4-node tetrahedron elements were also employed as the complex geometry required. The generation of the femur resulted in 245 elements for cartilage, 962 elements for cortical bone, 244 elements for subchondral bone, and 1726 elements for trabecular bone. The mesh generation of the tibia resulted in 222 elements for cartilage, 74 elements for cortical bone, 306 elements for subchondral bone, and 500 elements for trabecular bone. The menisci matrices were modeled by 424 8-node brick elements and their fibers 1212 nonlinear spring (combin39) elements, with 60 spar (link8) elements for attachments to the tibia. Nonlinear spring elements were used to simulate the collagen network throughout the menisci. Behavior of these elements was described by a force-deformation relationship, allowing both tension and compression. The ligaments were modeled by 30 nonlinear spring elements allowed to only undergo tension. The patella was modeled by 49 8-node brick elements [Figure A12], but was omitted from analysis, due to its negligible effect on axial loads in the knee.

Contact Problem

The frictionless nonlinear contact problem of articulation was modeled with 5-node (contac49) point to surface elements [Figure A13]. Contact was described between six articulating surfaces. These are the medial femoral condyle against the proximal medial meniscus, medial tibial condyle against the medial distal meniscus, and the medial

femoral condyle against the medial tibial condyle. The last three are similar on the lateral side. The convex surface of the distal femoral condyle were used as contactor points against the more concave target surface of the proximal menisci and tibial condyles. The distal menisci surfaces were considered as targets against the contactor tibial condyles. For each point on a contact surface, contact pair elements were generated for the closest nine rhombic target surfaces. A total of 3294 contact elements were automatically generated in this fashion. Images of the completed mesh are displayed [Figures A14, A15].

Material Properties

A linear elastic constitutive model was applied to the bone and cartilage elements in the model. The articular cartilage layers were modeled as isotropic with an elastic modulus (E) of 12 MPa and Poisson ratio (ν) of 0.45. These values compare with similar previous studies [Brown TD, et al. 1983; Haynes WC, et al., 1971; Haynes WC, et al., 1972]. To represent the fiber reinforced composite menisci, an elastic modulus of the matrix was chosen at 8 MPa. A Poisson ratio of 0.45 was used for this matrix. This approximates measurements taken from the cadaveric knee [Bendjaballah MZ et al., 1995].

Following previous published data [Carter DR, et al., 1978; Reilly DT, et al., 1974], the cortical bone elements were assigned properties of $E = 17000$ MPa, and $\nu = 0.3$.

Trabecular bone elements were given $E = 800$ MPa and $\nu = 0.4$ [Gibson, LJ 1985; Gibson, LJ 1988; Goldstein SA, 1987]. Subchondral bone elements were assigned $E = 8000$ MPa and $\nu = 0.3$. Table 1 summarizes the material properties of the components of the model.

Boundary Conditions

The model was tested in the ANSYS GUI under different loading conditions and constraints. Batch files were written in order to apply these conditions. Again, the patella was omitted from analysis for simplicity. With hopes of verifying the model with

Table 1: Material Properties Summary

Component	E (MPa)	ν	Element Type	Number of Elements
Cartilage	12	0.45	Solid45	515
Meniscus				
Body	8	0.45	Solid45	424
Fibers	*	*	Combin39	1212
Cortical Bone	17000	0.3	Solid45	1036
Trabecular Bone	800	0.4	Solid45	6827
Subchondral Bone	8000	0.3	Solid45	551
Ligament	*	*	Combin39	35
Contact	*	*	Contac49	3294

* Nonlinear components are not defined through E and ν .

experimental results to follow, the boundary conditions were set to mimic experimental loading. At the same time we would like to predict the knee motions at different constraint conditions so that we could design our experimental fixtures to simulate an in-vivo knee motions. In this case the finite element analyses of our model and future experimental analyses will complement each other. In general, the proximal nodes on the femur are constrained. The first fixation method attempted was to fix displacement in the anterior-posterior and medial-lateral plane (Constrained Model) [Figure 4]. This was intended to allow only axial compression of the joint (z direction), without translation or rotation on x-y plane. The second method attempted was to couple the axial degree of freedom (Coupled Model) [Figure 5]. This requires that all the nodes on the proximal surface of the femur to move in concert. A fixation of this sort allows for translation in the medial-lateral, anterior-posterior, and axial degrees of freedom. It also allows for varus - valgus rotation as well as translation in x-y plane.

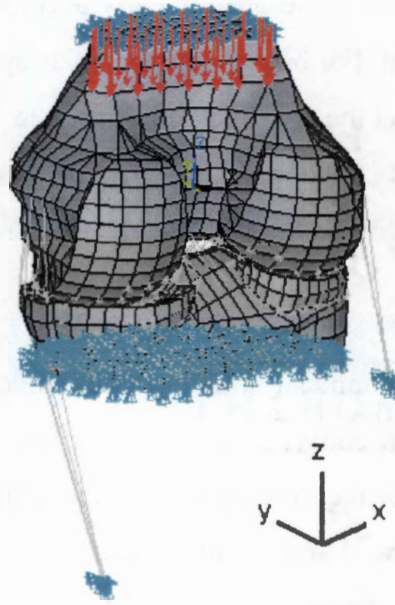


Figure 4: Boundary Conditions Applied to Constrained Model
(Describes fixation to only allow translation in z direction)

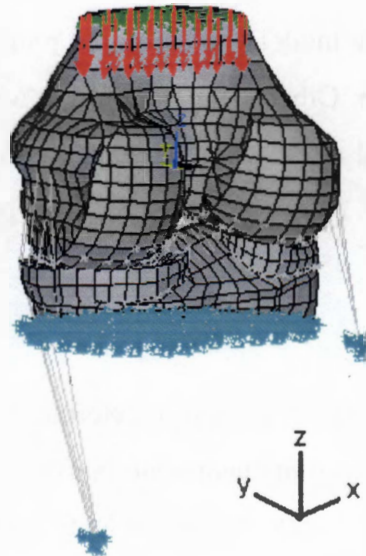


Figure 5: Boundary Conditions Applied to Coupled Model
(Describes fixation to allow rotation about z and translation in x, y, and z directions)

The second method was deemed more anatomically accurate, since it would allow the joint to settle as load is applied. For both cases, load was applied in the distal direction, normal to the transverse plane at the proximal femur surface. The distal tibial surface was constrained in all degrees of freedom. This prevented any rotation or translation, simulating a rigid connection with an experimental loading fixture.

Nonlinear Analysis Parameters

As a complicated and highly nonlinear structure, this model has many parameters that must be set in ANSYS to allow convergence. Initial values were chosen to allow simple convergence. These values may require change in future studies involving this model as time and new conditions allow. Large displacement static analysis was considered to allow translation of the model. Time at end of loadstep was set to 1000 to correspond to the total applied load of 1000 N that was attempted. Automatic time stepping was set to program chosen, with substeps allowed to range in number from 50 to 500. Results were recorded for every second substep reaching convergence. The default program chosen equation solver was allowed in effort to speed solution. Maximum number of equilibrium iterations was set to 60, since the model often required more than the default 27 to reach convergence for a given substep. Other solution controls were also left to their defaults. Initial parameters were assigned to the contact elements to allow solution as well. The contact stiffness was set to 1000. Penetration tolerance and pinball radius were set to 0.01 and 3.0 respectively.

Modal Analysis Parameters

Modal analysis was performed on both models to determine the natural frequencies of vibration. Densities of the various component materials of the knee were also assigned initial values as follows [Table 2]. Since the unit of length used in generating the model was millimeters, density had to be specified in Mg/mm. This required a conversion from g/cm^3 to Mg/mm^3 by multiplying the original density by 10^{-9} . The knee was lightly

Table 2: Density of Materials

Component	Density (g/cm ³)
Cortical Bone	1.85
Trabecular Bone	0.3
Subchondral Bone	1.85
Cartilage	0.8
Meniscus	0.8

preloaded with 100 N and nonlinear static analysis was performed. Block-Lanczos modal analysis was performed to extract the first six modal frequencies and mode shapes, including prestress effects of static loading. The effect of upper body mass was disregarded in this study.

Chapter 3: Results

Nonlinear static analysis and modal analysis was conducted to verify that the finite element model was functioning as expected. For the static analysis, two methods of proximal femur fixation were examined. Loading was applied to the point of simple convergence. For greater loading, additional work will be required to optimize the nonlinear properties of the model. This is intended for future research. The results of the static analysis are displayed [Figure 6]. There appears to be a slight stiffening effect in the curves around 50 N loading. This may result from the contact elements engaging after an initial displacement or tension in the ligaments reaching a linear threshold.

In order to present examples of similar loading cases, the time step corresponding to 182.5 N loading was selected from the solution of the constrained model, and the time step corresponding to 168 N was selected from the coupled model solution. Von Mises stress plots and deformed mesh plots were produced for the components of interest.

Deformation

The maximum total deformation was found to be less for the constrained model [Figure 7], with 1.828 mm vs. 2.98 mm for the coupled model [Figure A15]. It was also noticed that the coupled model underwent not only simple axial deformation, but also axial rotation and translation. The constrained model was prevented from experiencing anything but axial deformation due to its boundary conditions. The displacement results for the tibia were found to be slightly greater in the constrained model [Figure A16], with 0.30 mm than in the coupled model [Figure A17], with 0.19 mm displacement. For each, the greatest nodal displacement took place on the tibial condyles. The femur experienced large displacement in both models [Figures A19, A20] including rigid body motion in the direction of loading. Also, the maximum nodal displacements in the model took place in the femur.

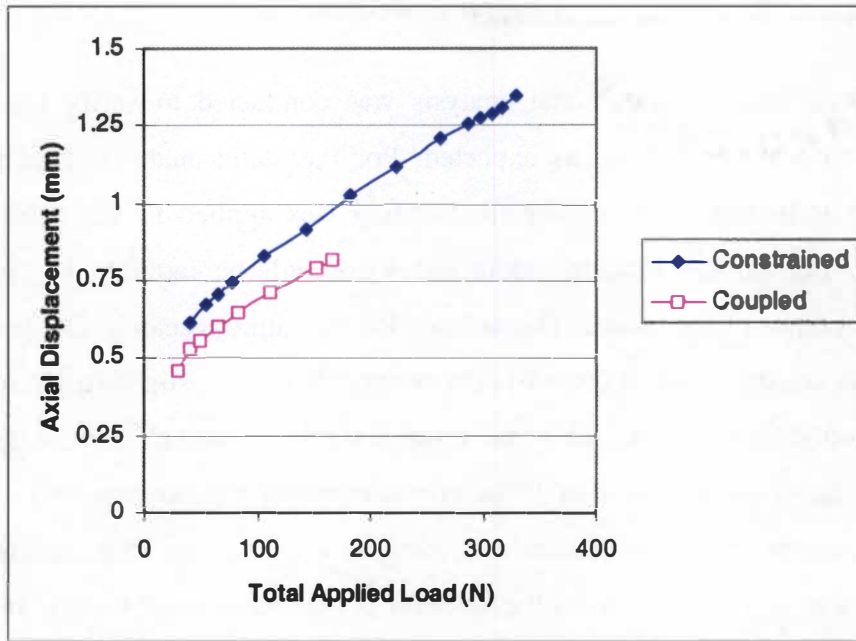


Figure 6: Axial Femoral Displacement vs. Total Applied Load

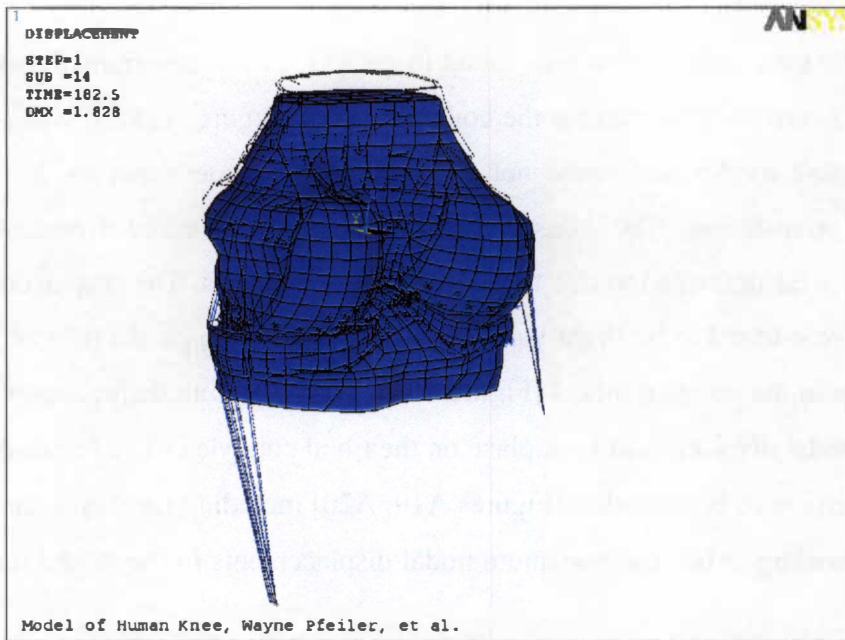


Figure 7: Displacement of Entire Constrained Model
(Dashed lines show original position of model. Blue shows deformed shape.)

The meniscus also experienced large deformations, 1.19 mm in the constrained model [Figure A21] and 1.5 mm in the coupled model [Figure A22]. More deformation was present on the medial side of the meniscus in both models.

Stress Distribution

To illustrate the difference in stress distribution, von Mises stress plots were created for both models [Figures 8, 9]. Plots were rotated to best illustrate the maximum stress and recorded. The Constrained Model femoral cartilage [Figure A23] showed a maximum stress in the medial condyle, while the Coupled Model [Figure A24] generated a maximum at the lateral condyle. The difference in stress was notable, with 2.57 MPa in the Constrained Model and 0.75 MPa in the Coupled Model. The tibial cartilage presented similar stress plots for both models [Figures A25, A26], with local maxima on the lateral condyles. Plots of the meniscus [Figures A27, A28] show similar relative stress distributions, but the lateral half of the Constrained Model [Figure A29] received roughly twice the maximum stress of the Coupled Model [Figure A30]. The medial meniscus experienced greater stress in the Coupled Model [Figure A31] than in the Constrained Model [Figure A32], but both maxima were located at the anterior horn. Although the maximum-recorded stresses in the femur of both models were very similar in magnitude, the locations were varied. The Constrained Model [Figure A33] experienced a maximum inside the intercondylar notch, while the Coupled Model [Figure A34] took a maximum at the lateral proximal cortical shell. The tibia in both models [Figures A35, A36] presented similar stress plots, both in value and distribution, with maxima at the subchondral connection to the lateral meniscus. The femoral subchondral bone plots revealed a variance in distribution between the two models. The Constrained Model [Figure A37] showed a maximum just anterior of the intercondylar notch while the coupled model [Figure A38] showed a maximum at the lateral side.

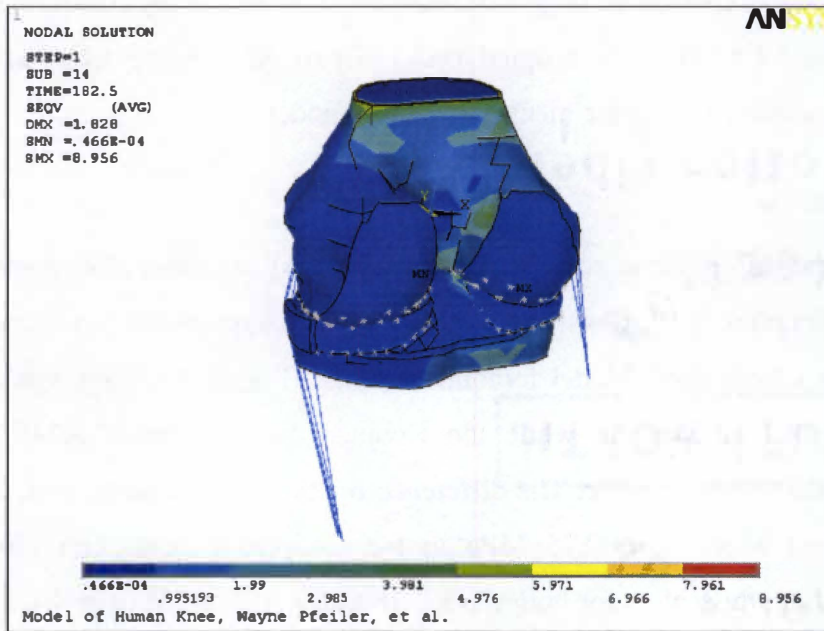


Figure 8: Stress Distribution in Entire Constrained Model
(Dark blue represents lowest stress)

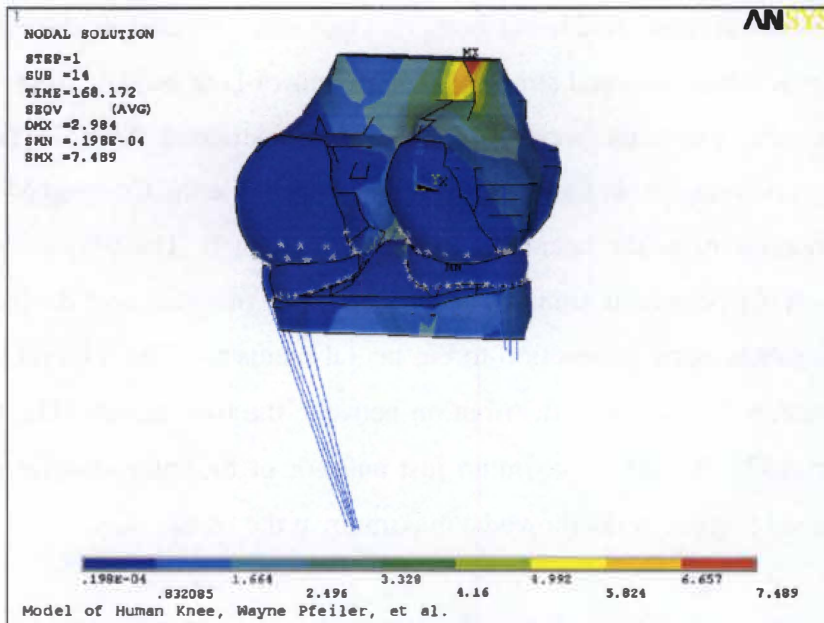


Figure 9: Stress Distribution in Entire Coupled Model

The tibial subchondral bone showed similar stress plots between both models [Figures A39, A40], with concentrations at the lateral side of the intercondylar prominence. The femoral cortical shell of each model revealed the maximum stress associated in the femur, with a maximum of the Constrained Model [Figure A41] at the center of the anterior intercondylar notch, and a maximum stress of the Coupled Model [Figure A42] at the proximal lateral femoral shaft. The femoral trabecular bone presented the greatest stress on the medial edge of the intercondylar notch in the Constrained Model [Figure A43], and the Coupled model gave a maximum at approximately the same location on the lateral side [Figure A44]. Finally, the tibial trabecular bone in both models showed maxima at similar locations, both on the medial side of the intercondylar prominence [Figures A45, A46].

Modal Analysis

Modal analysis was performed on both models to determine the first six natural frequencies of vibration. The results are listed below [Table 3]. Animations of mode shapes were created and the extreme displacements of each were recorded, with example below [Figure 10] and others in Appendix [Figure A47 to A57]. The axial compression modes show displacement along the z-axis. Other modes show rotation and translation in other directions. The modal frequencies of the Constrained Model were in general higher than the frequencies for the Coupled Model, probably due to the greater stiffness imposed by the boundary conditions.

Table 3: Frequencies and Mode Shapes

Model	Mode Number	Frequency (Hz)	Description
Constrained	1	10.619	Axial compression
	2	35.780	Torsion about Y-axis
	3	79.647	Torsion about X-axis
	4	240.12	Warping
	5	244.30	Warping
	6	261.58	Trabecular bone oscillation
Coupled	1	2.5505	Torsion about z
	2	5.9778	Torsion about z
	3	7.7613	Compression, translation
	4	17.702	Axial compression
	5	126.26	Torsion, warping
	6	127.73	Warping

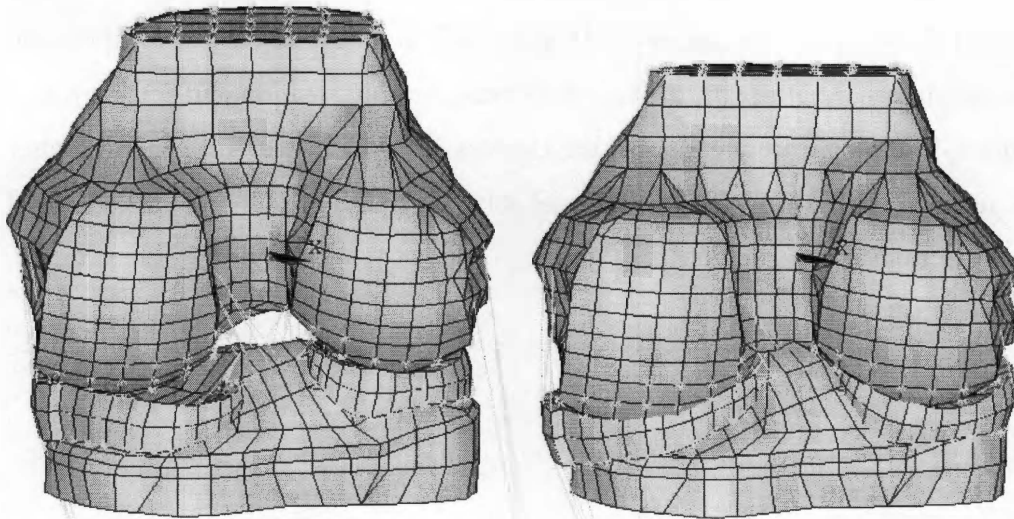


Figure 10: Mode 1 of Constrained Model
(Showing axial compression)

Chapter 4: Discussion

In this study a detailed nonlinear dynamic finite element model of the human knee joint was developed. The model was analyzed under static loading at different constraint conditions. The top Constrained Model converged at 330 N, while the top Coupled Model converged at 168 N. Modal analyses were performed to find mode shapes. The mode shapes are one of the basic dynamic characteristics of any structure.

Clinical Application of the Model

By including the upper body mass, this study is the first of its kind to give us valuable information about changes in basic dynamic characteristics of the knee joint. For example, our future parametric analyses will show the critical combinations of dynamic amplitude, preload, and upper body mass that can lead to high stresses at the joint leading to OA. Therefore, by referring to the resulting data, preventive measures can be determined for different activities involving different combinations of preload, body mass, and dynamic amplitude. This can apply to different sport and occupational activities. In this case, the chance of developing OA in an individual with a certain body mass and certain habits of performing sport or occupational activities may be predicted. Knowing how the changes in the body mass can affect the joint dynamic behaviour, the preventive measures or rehabilitation exercises can be designed. The finite element model can simulate many clinical scenarios. Furthermore, advancement of this study should produce reference data, which is essential for researchers, clinicians, and bioengineers in their research and design projects dealing with the effect of mechanical factors in causation, prevention and rehabilitation of osteoarthritis. The proper treatment, prevention and rehabilitation strategies as well as improvement in design of prostheses cannot be achieved without understanding the basic dynamic characteristics of the knee joint. Without referring to the dynamic system parameters data and their changes under different body mass and loading conditions, efforts in the design of new rehabilitation

and preventive techniques may be wasted or timely to achieve. Injury or disease may be modelled by removing the elements corresponding to a ligament, or altering the modulus of trabecular bone to correspond to the osteoporotic case. Hence, comparisons may be made with the normal knee analysis in order to design bracing that may delay damage to the newly vulnerable tissues. Novel surgical procedures that alter the anatomy of the knee might be modelled in order for physicians to understand the effect of the procedure before they operate.

Nonlinear Analysis

The highly nonlinear properties of the finite element model caused great difficulties in convergence. Much time and effort was spent trying to optimize variables to yield a converged system obtain valid results. The contact problem was the first major obstacle to overcome in analysis. In early versions of the model, the pinball radius (a control parameter) [ANSYS, 1997, 2003] had been set too small, due to a misunderstanding of its purpose. This pinball radius defines a spherical region around the contact node. When a target surface is found to fall within this region, the condition of contact is considered and extra calculations are preformed. In this fashion, ANSYS optimizes calculation time. The problem that resulted from the prior misunderstanding of the pinball region is that rigid body motion was occurring and the femur was effectively falling through the tibia. This happened because there is a small initial gap between contacting surfaces in the model, and the contact elements never engaged. This problem was solved by increasing the pinball radius, so that the condition of contact would be considered from the very beginning of analysis. Many of the other difficulties in convergence deal with altering similar variables. Since the model is very large, and the solution is very complex, this will continue to be an issue that must be addressed as the model is used to perform additional analyses. The main problem seems to be the large deformation of menisci causing too much distortion in the contact element therefore causing difficulties to reach convergence.

Deformation in Static Loading

From the results listed previously, it was noted that the two models experienced different deformations and rigid body motions, as would be expected. The meniscus had large deformations on the edges that were not constrained by geometry. This is probably an oversimplification of the knee, since mesenchymal attachments would limit the motion of these bodies. Perhaps future studies will add this to the model. Some of the displacements along the inner edges of the meniscus are suspect, since the loading appears concentrated around the contact points of the femoral condyle, instead of being evenly distributed. This may be due to a parameter of the contact elements and should be investigated further. The Coupled Model rotated axially, equivalent to a slight valgus rotation. The Constrained Model was prevented from any rotation by its boundary conditions. Because of this difference, the Coupled Model tended to distribute load more evenly over the cartilage surfaces by allowing the condyles to settle into their proper alignments. The Constrained Model tends to force an unnatural loading condition by not allowing this settling to take place. In this way, the Coupled Model comes closer to modeling the true physiology of the knee. It is hoped that future work will focus on this version of the model, unless another purpose exists to unnaturally constrain the knee.

Modal Analysis

The frequencies of axial compressive modes were of particular interest, since they would be used as a reference for a future experimental study. These modes were found to exist around frequencies from 7.7 to 17.7 Hz, depending on boundary condition. The 17.7 Hz result compares favorably with a previous experimental study [Jans et al., 1988]. That study reported the resonant frequency of a knee joint in the axial direction without an upper body mass to be about 20-30 Hz. The higher modes of each model experienced warping of the femoral shaft, which is due to the boundary conditions imposed. Future studies may further restrict motion on this surface and eliminate those warping modes.

Future Work

Since the development of this model was intended to be the initial step in a series of analyses and experiments, we have several intentions for the future of this project. The first of the plans is to verify the model with an experimental dynamic study of the human knee. We intend to examine the possibility of altering the characteristics of the meniscus in order to better simulate the sudden or large magnitude impacts on the knee. We also intend to simulate different clinical conditions to see what vulnerabilities might exist in the knee. In summary, this model is intended as a tool to enable further detailed research on the human knee.

List of References

Abdel-Rahman E, Hefzy MS. "Three dimensional dynamic modeling of the tibio-femoral joint." *Advances in Bioengineering ASME*. 1993; BED-26: 315-318.

ANSYS Expanded Workbook. Release 5.4. Canonsburg, PA, 1997.

ANSYS Release 8.0 Documentation. Canonsburg, PA, 2003.

Bendjaballah MZ, Shirazi-Adl, A, Zukor, DJ. "Finite element analysis of human knee joint in varus-valgus." *Clinical Biomechanics*. 1997; 12: 139-148.

Bendjaballah MZ, Shirazi-Adl A, Zukor DI. "The biomechanics of human knee joint in compression: reconstruction, mesh generation and finite element analysis." *The Knee*. 1995; 2: 69-79.

Bendjaballah MZ, Shirazi-Adl, A, Zukor, DJ. "Biomechanical response of the human knee joint under anterior-posterior forces." *Clinical Biomechanics*. 1998; 13: 625-633.

Blankevoort L, Kuiper JH, et al. "Articular contact in a three-dimensional model of the knee." *Journal of Biomechanics*. 1991; 24: 1019-31.

Brown TD, Digionia AM, et al. "A contact coupled nonlinear finite element analysis of the hip joint." *Trans 29th Annual Meeting ORS*. 1983; 8: 66.

Carter DR, Spengler DM. "Mechanical properties and composition of cortical bone." *Clinical Orthopedics*. 1978; 135: 192-217.

Cooper C. "Occupational activity and the risk of osteoarthritis." *Journal of Rheumatology Supplement* 1995; 43: 10-12.

Dieppe P. "Strategies for the prevention of osteoarthritis." *Internal Journal of Tissue Reaction*. 1993; 15(3): 93-7.

Felson DT. "Weight and osteoarthritis." *American Journal of Clinical Nutrition*. March 1996; 63(3 Supplement): 430S-432S.

Felson DT, Chaisson CE. "Understanding the relationship between body weight and osteoarthritis." *Baillieres Clinical Rheumatology*. November 1997; 11(4): 671-81.

Felson DT, Naimark A, Anderson J, Kazis L, Castelli W, Meenan RF. "The prevalence of knee osteoarthritis in the elderly. The Framingham Osteoarthritis Study." *Arthritis and Rheumatism*. August 1987; 30(8): 914-8.

Freeman MAR. "How the knee moves." *Current Orthopaedics*. December 2001; 15(6): 444-450.

Gibson, LJ. "Cancellous bone." *Cellular Solids*. 1988; 316-331.

Gibson, LJ. "The mechanical behavior of cancellous bone." *Journal of Biomechanics*. 1985; 18: 317-328.

Gill HS, O'Connor JJ. "Biarticulating two-dimensional computer model of the human patellofemoral joint." *Clinical Biomechanics*, March 1996; 11(2): 81-89.

Goldstein SA. "The mechanical properties of trabecular bone: Dependence on anatomic location and function." *Journal of Biomechanics*. 1987; 20: 1055-1061.

Gray's Anatomy. Thirty-eighth Edition. New York, 1995.

Haynes WC, Keer LM, et al. "A mathematical analysis for indentation tests of articular cartilage." *Journal of Biomechanics*. 1972; 5: 541-51.

Haynes WC, Mockros LF. "Viscoelastic properties of human articular cartilage." *Journal of Applied Physiology*. 1971; 31: 562-8.

Hirokawa S. "Three dimensional mathematical model analysis of the patellofemoral joint." *Journal of Biomechanics*. 1991; 24: 659-71.

Holibkova A, Machalek L, Holibka R, Ghromek Z. "Lisions of the knee joint menisci in miners." *ACTA Universitatis Palackianae Olomucensis Facultatis Medicae*. 1989; 123:147-68.

Jans H, Dortmans L, Sauren A, et al. "An experimental approach to evaluate the dynamic behavior of the human knee." *Journal of Biomechanics*. 1988; 110: 69-73.

Kirsch L, Kohn D, Glowik A. "Forces in medial and lateral meniscus sutures during knee extension - an in vitro study." *Journal of Biomechanics*. July 1998; 31(1): 104

Komistek RD, Northcut EJ, et al. "An in vivo analysis of osteoarthritic subjects walking with and without a knee brace." *Journal of Biomechanics*. July 1998; 31(S1): 32

March LM, Bachmeier CJ. "Economics of osteoarthritis: a global perspective." *Baillieres Clinical Rheumatology*. November 1997; 11(4): 817-34.

- Neyret P, Donell ST, Dejour H. "Osteoarthritis of the knee following meniscectomy." *British Journal of Rheumatology*. March 1994; 33(3): 267-8.
- Powell JW, Barber-Foss KD. "Injury patterns in selected high school sports: a review of the 1995–1997 seasons." *Journal of Athletic Training* 1999; 34(3): 277–284.
- Radin E.L., Parker H.G., Pugh J.W., Steinberg R.S., Paul, I.L. and Rose R.M. "Response of joint to impact loading- III." *Journal of Biomechanics*. 1973; 6: 51-57.
- Reilly DT, Burstein AH. "The mechanical properties of cortical bone." *Journal of Bone Joint Surgery*. 1974; 56: 1001-1022.
- Roos H. "Are there long-term sequelae from soccer." *Clinics in Sports Medicine*. 1998; 17: 819-831.
- Sandmark H, Vingard E. "Sports and risk for severe osteoarthrosis of the knee." *Maryland Medical Journal*. August 1996; 45(8): 644-7.
- Spector TD, Harris PA, et al. "Risk of osteoarthritis associated with long-term weight-bearing sports: a radiological survey of the hips and knees in female ex-athletes and population controls." *Arthritis and Rheumatism*. 1996; 39: 988-995.
- Thompson D, Edelsberg J, Kinsey KL, Oster G. "Estimated economic costs of obesity to U.S. business." *American Journal of Health Promotion*. Nov-Dec 1998; 13(2): 120-7.
- Van Eijden TMGJ, Kouwenhoven E, et al. "A mathematical model of the patellofemoral joint." *Journal of Biomechanics*. 1986; 19: 219-29.
- Wisman J, Veldpaus F, et al. "A three-dimensional mathematical model of the knee joint." *Journal of Biomechanics*. 1980; 13: 677-85.
- Wolfe F, Hawley DJ, Peloso PM, Wilson K, Anderson J. "Back pain in osteoarthritis of the knee." *Arthritis Care and Research*. 1996; 9: 376-383.

Appendix



Figure A1: Meniscus Body

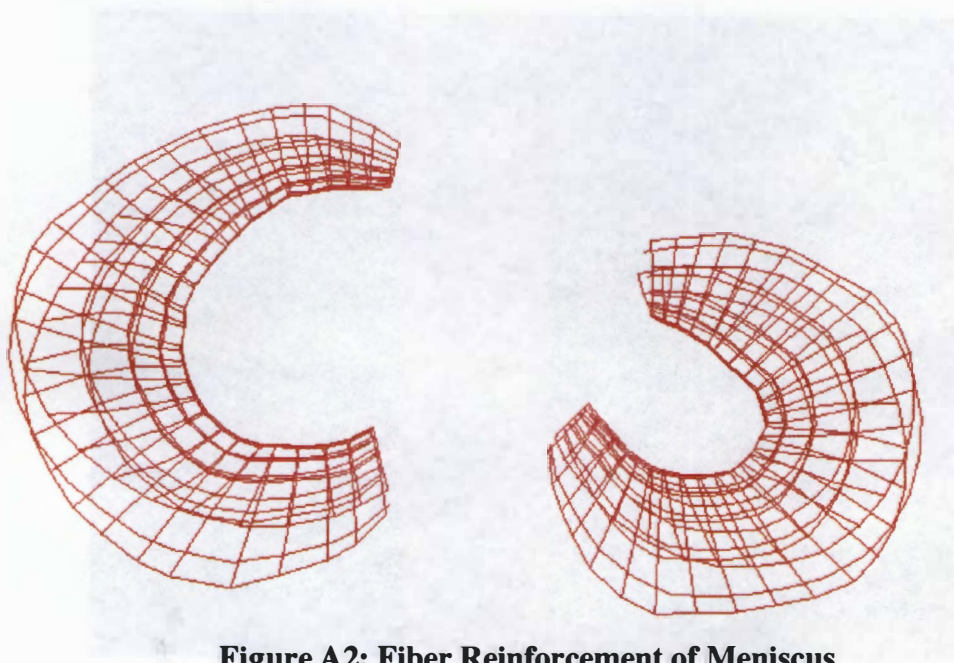


Figure A2: Fiber Reinforcement of Meniscus

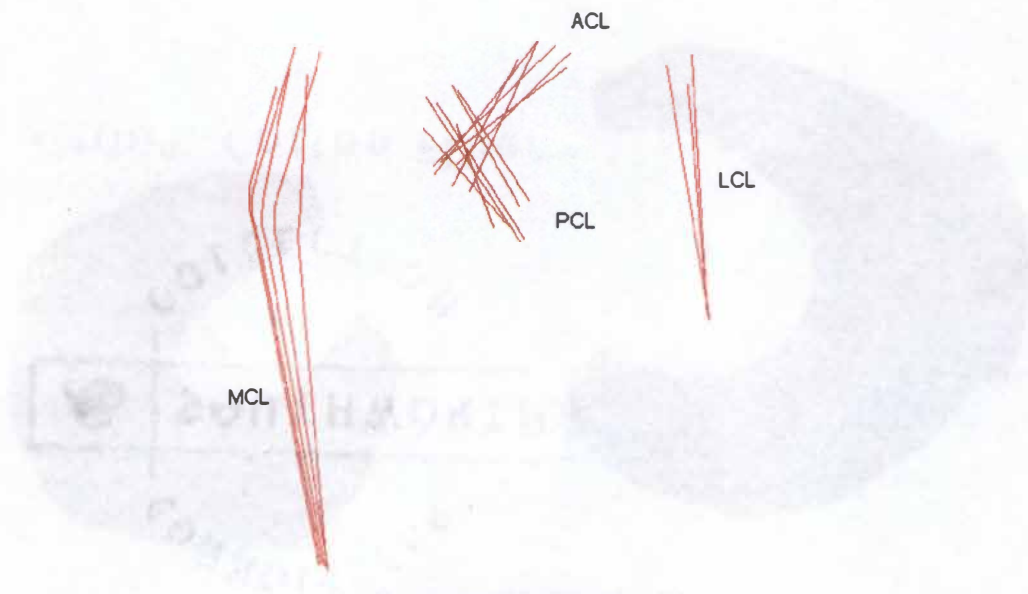


Figure A3: Ligaments

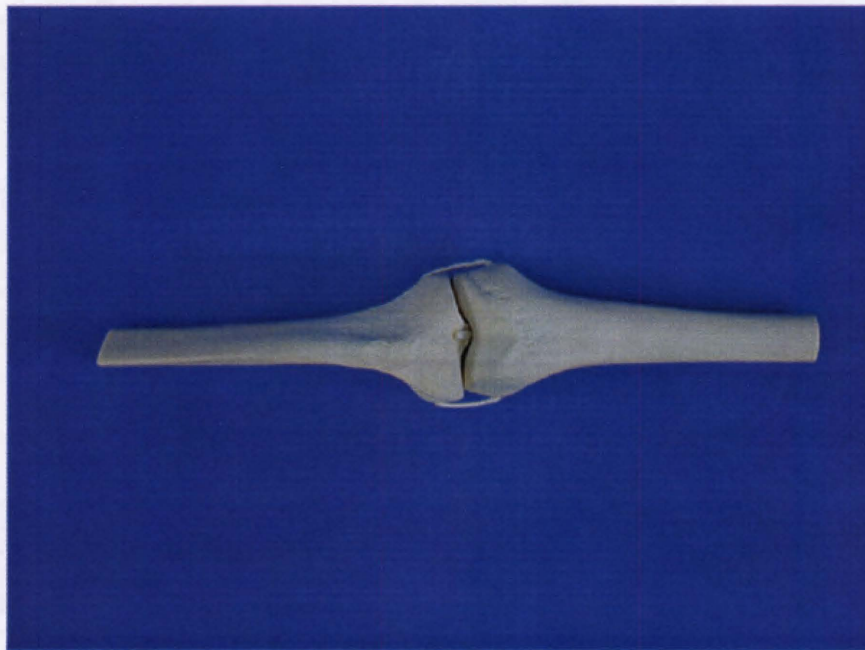


Figure A4: Original Sawbones Model of Knee
<http://www.sawbones.com/images/products/1/1152.jpg>

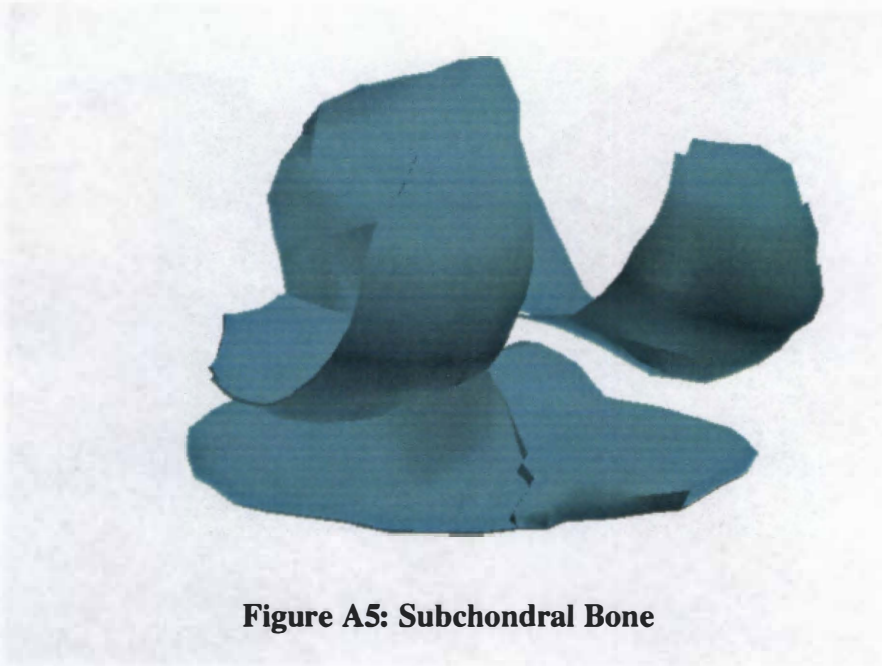


Figure A5: Subchondral Bone



Figure A6: Section Markings on Sawbones



Figure A7: Applying Magnet Wire to Sawbones

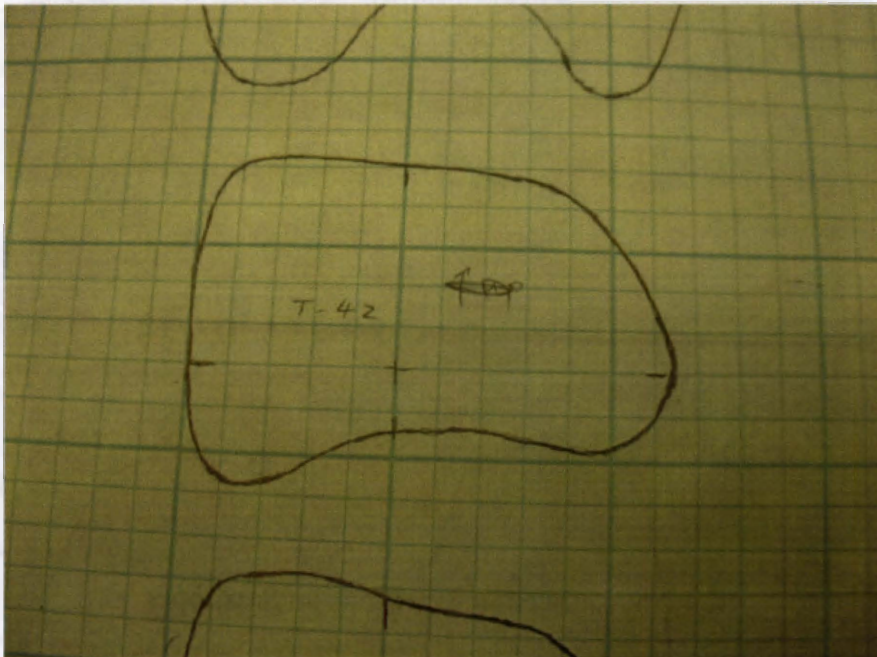


Figure A8: Traced Outline of Magnet Wire

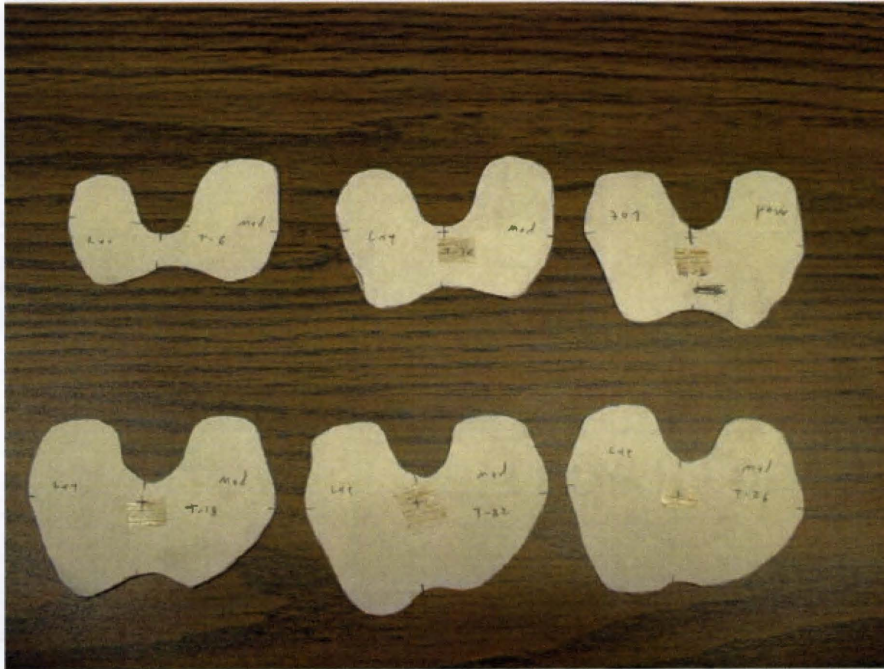


Figure A9: Profiles of Section Geometry



Figure A10: Cortical Bone

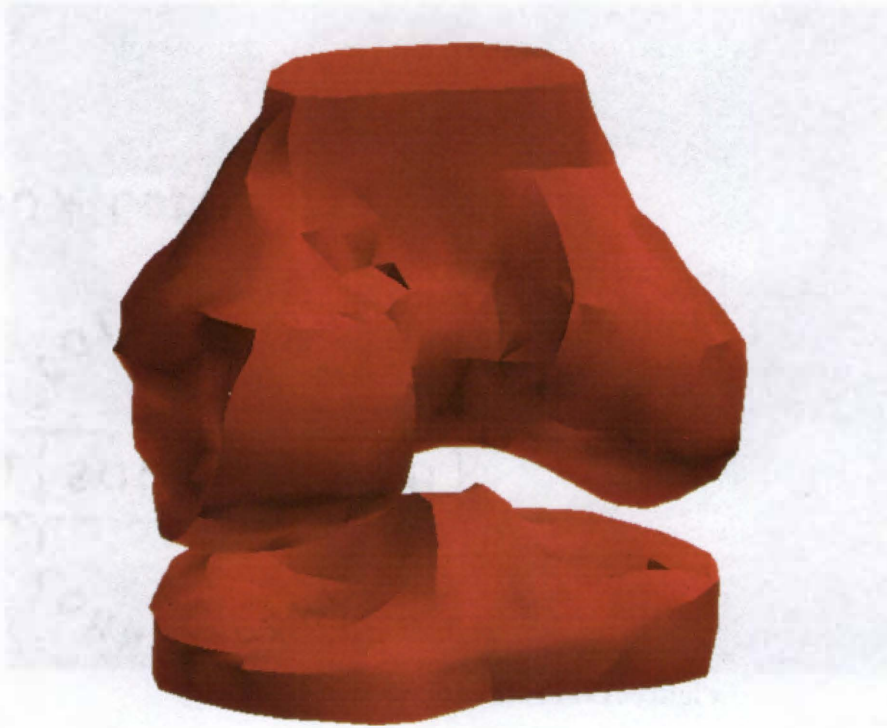


Figure A11: Trabecular Bone

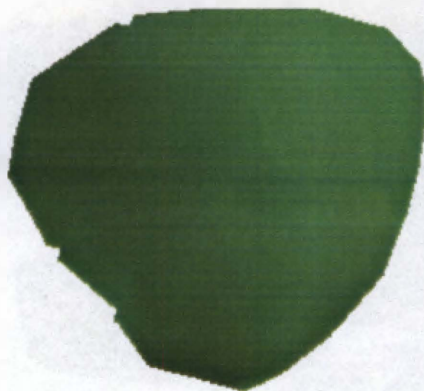


Figure A12: Patella



Figure A13: Contact Surfaces
(Contact nodes shown as stars, target surfaces displayed as solids.)

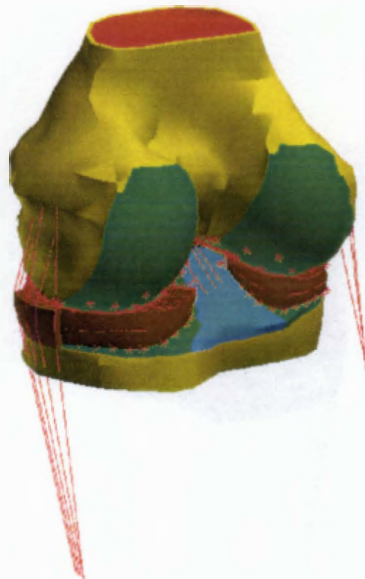


Figure A14: Completed Model, Posterior View

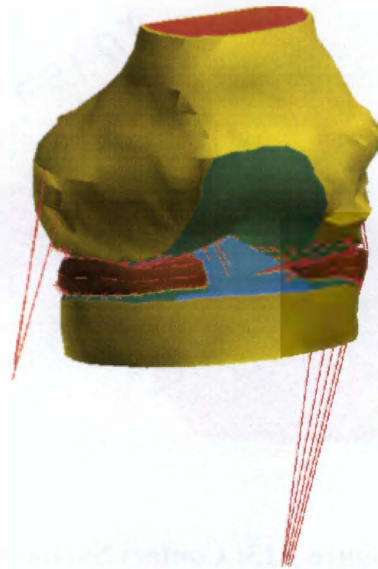


Figure A15: Completed Model, Anterior View

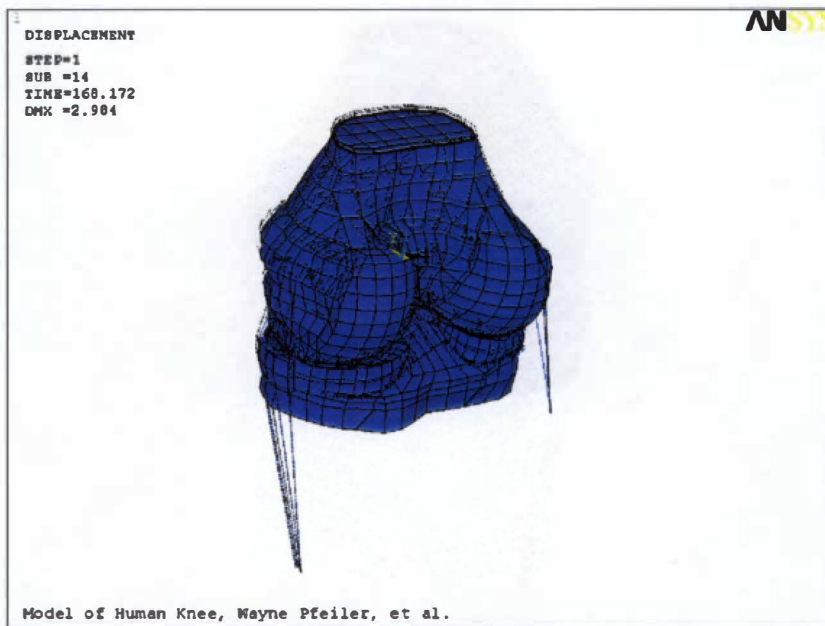


Figure A16: Displacement of Entire Coupled Model

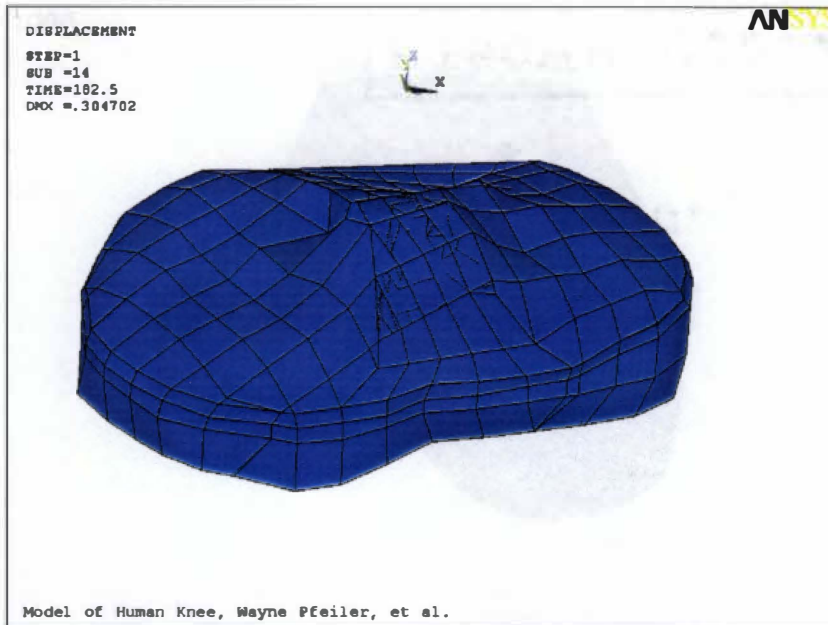


Figure A17: Displacement of Constrained Model Tibia

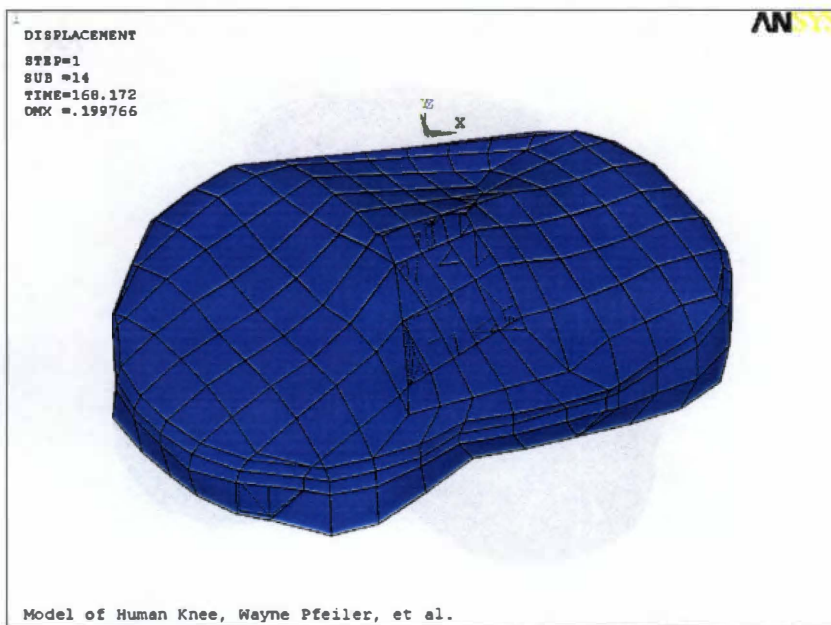


Figure A 18: Displacement of Coupled Model Tibia

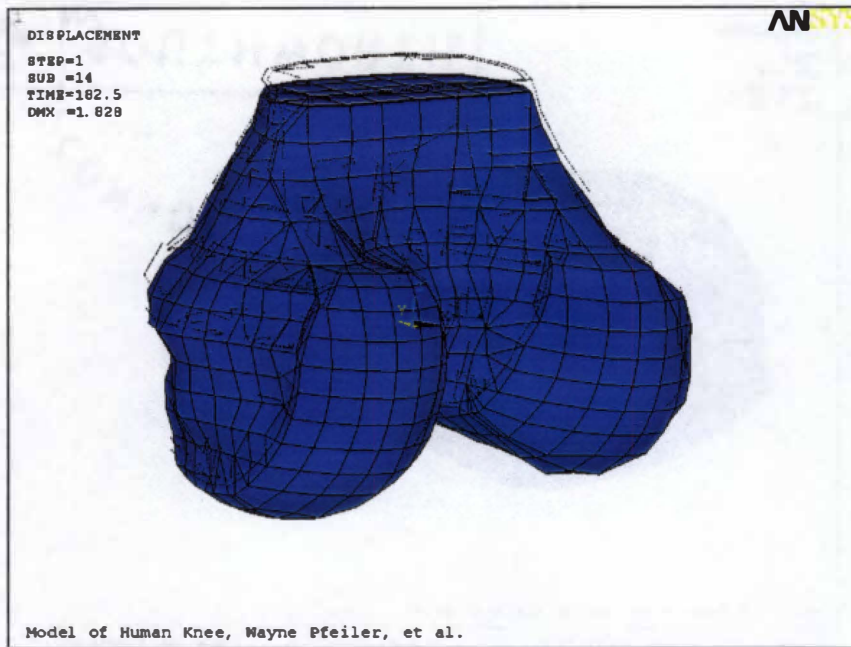


Figure A19: Displacement of Constrained Model Femur

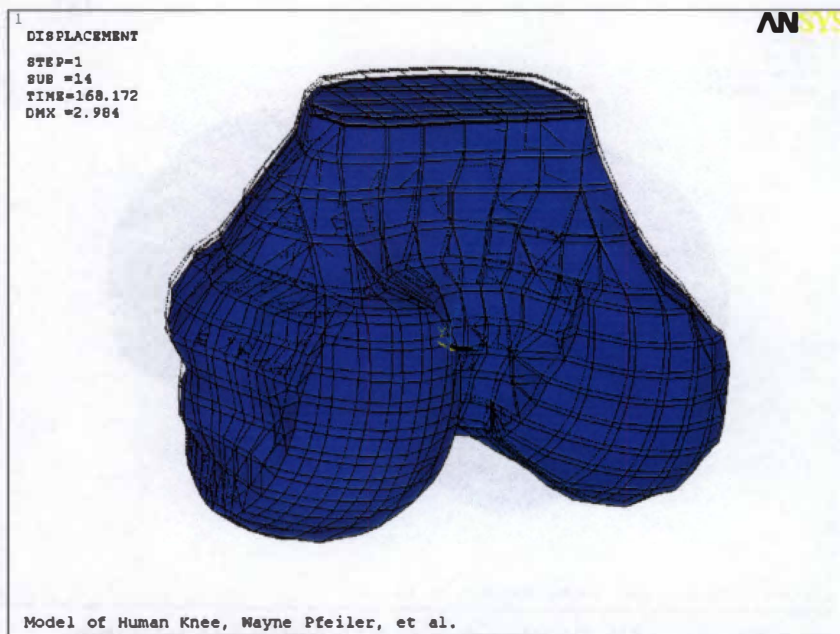


Figure A20: Displacement of Coupled Model Femur

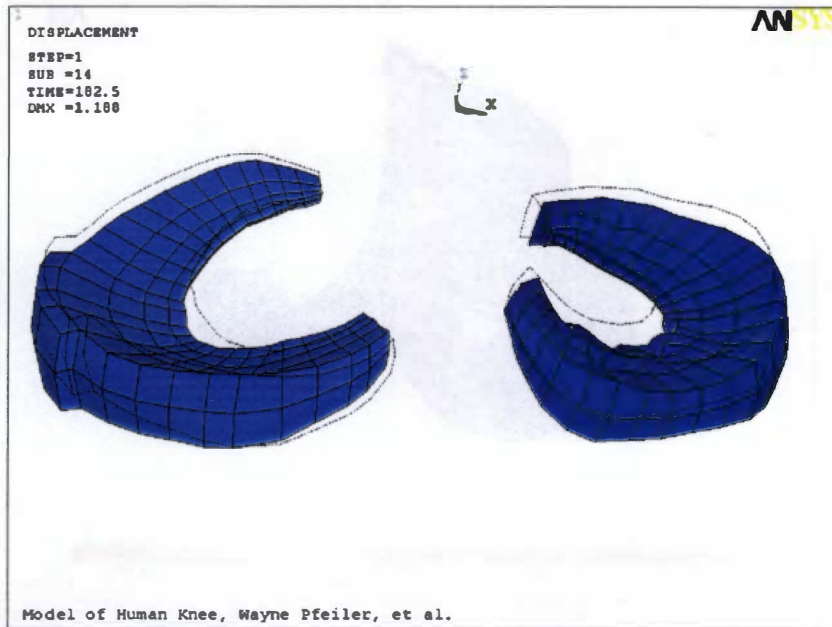


Figure A21: Deformation of Constrained Model Meniscus

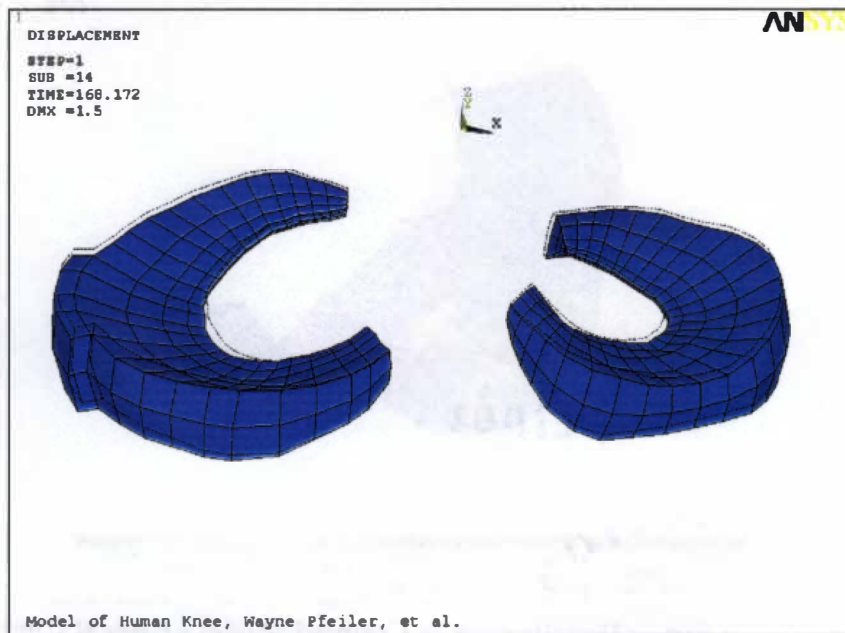


Figure A22: Deformation of Coupled Model Meniscus

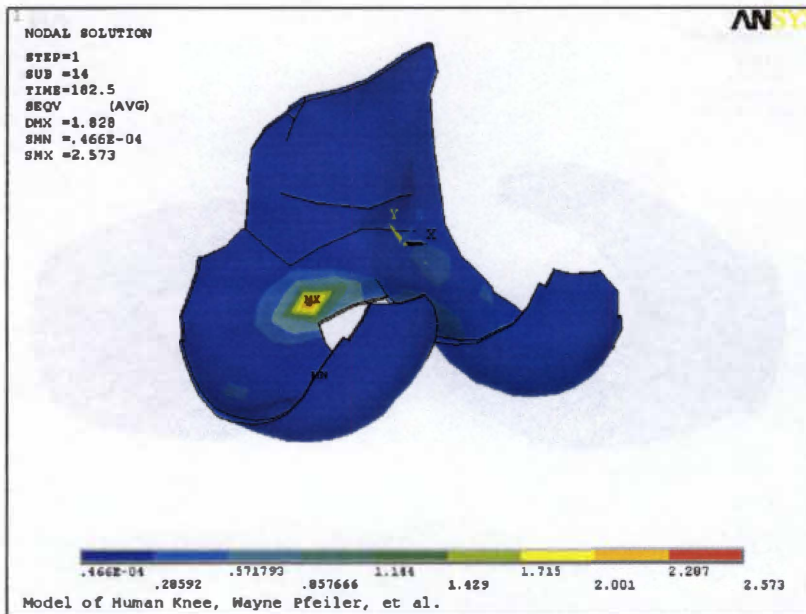


Figure A23: Stress Distribution in Constrained Model Femoral Cartilage

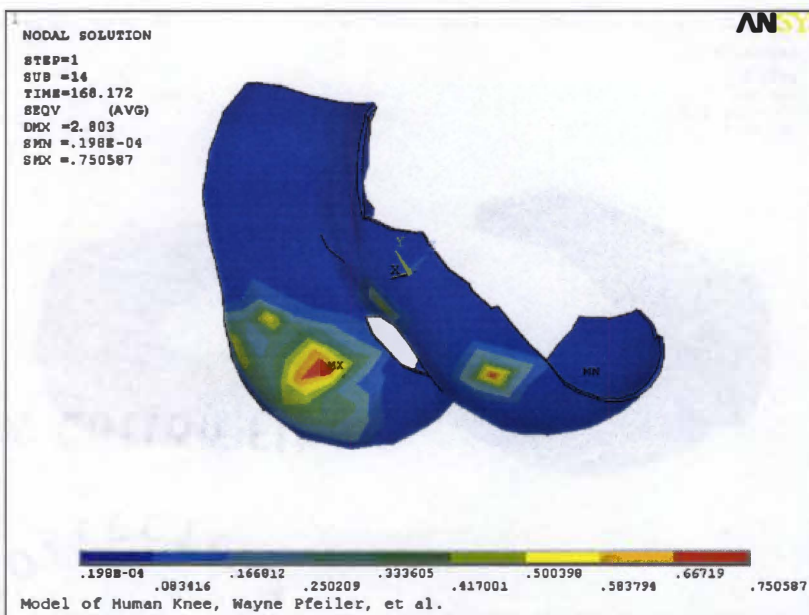


Figure A24: Stress Distribution in Coupled Model Femoral Cartilage

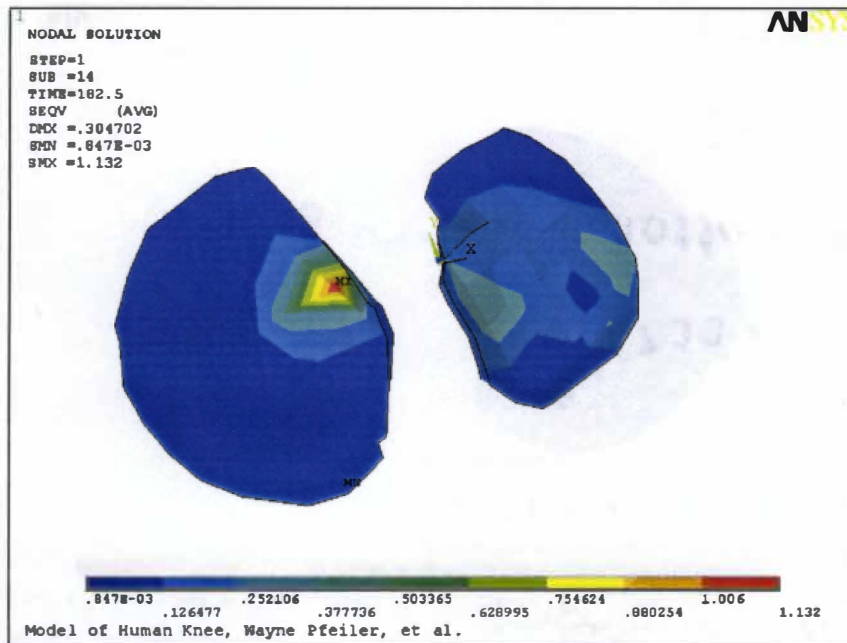


Figure A25: Stress Distribution in Constrained Model Tibial Cartilage

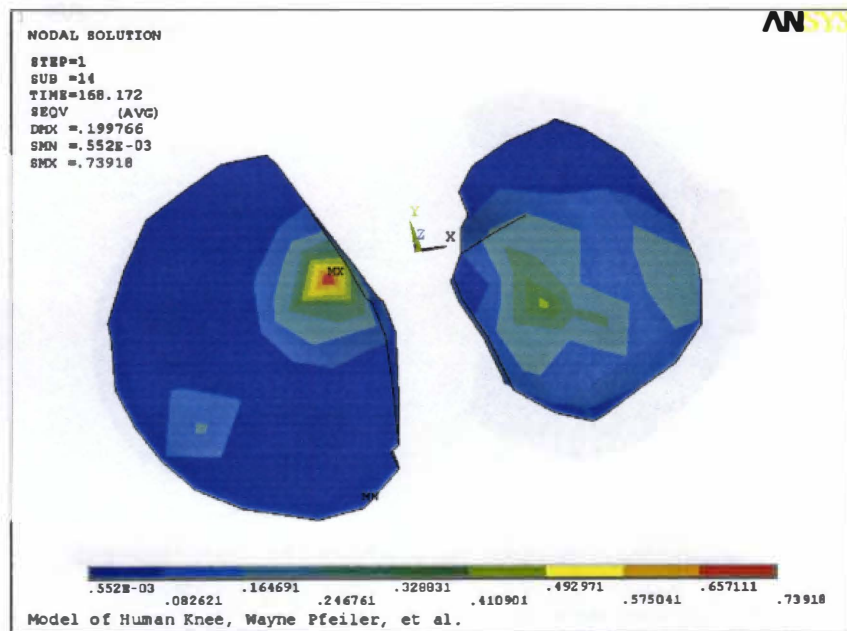


Figure A26: Stress Distribution in Coupled Model Tibial Cartilage

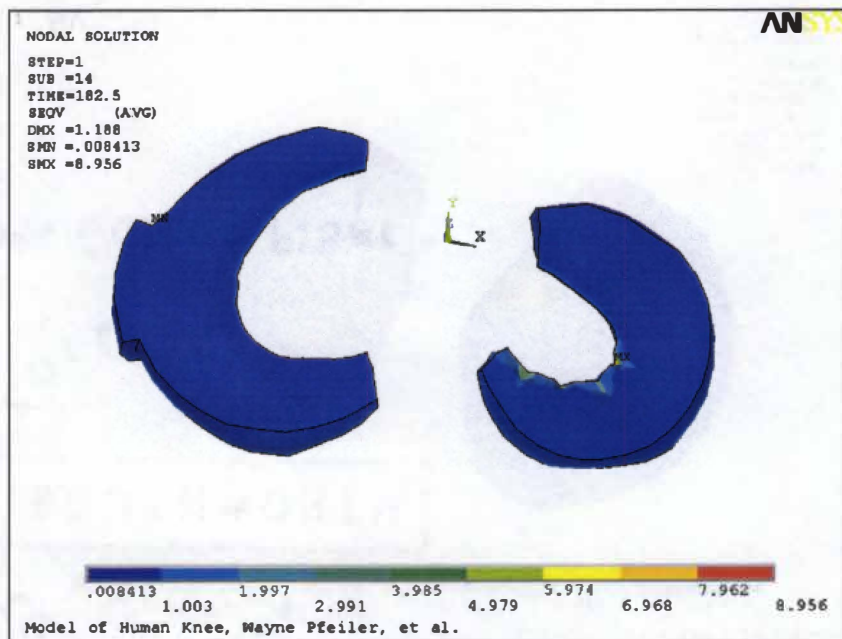


Figure A27: Stress Distribution in Constrained Model Meniscus

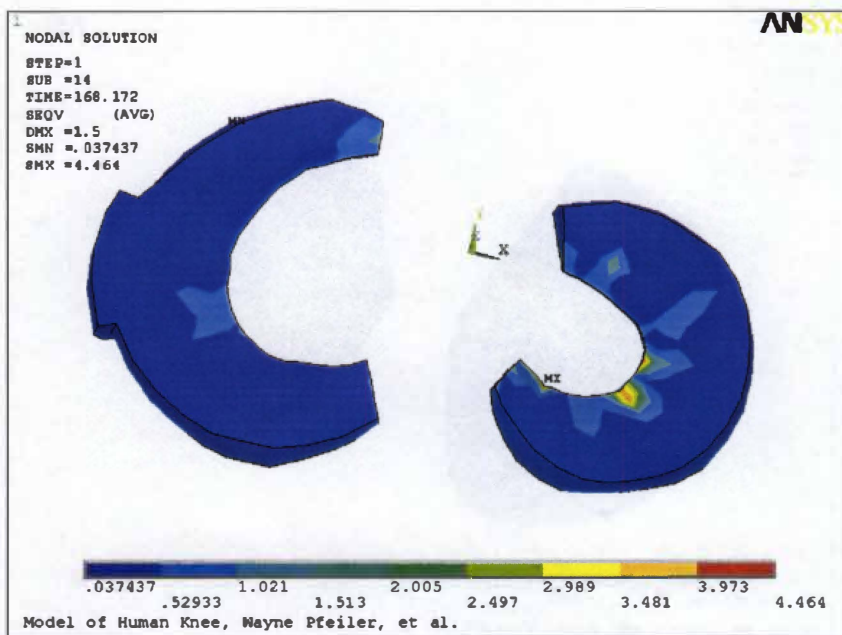


Figure A28: Stress Distribution in Coupled Model Meniscus

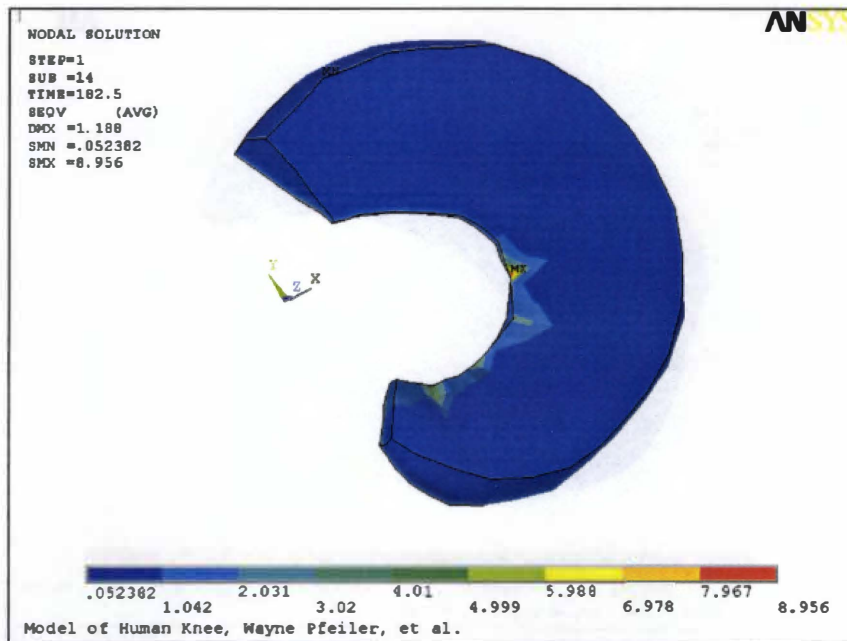


Figure A29: Stress Distribution in Constrained Model Lateral Meniscus

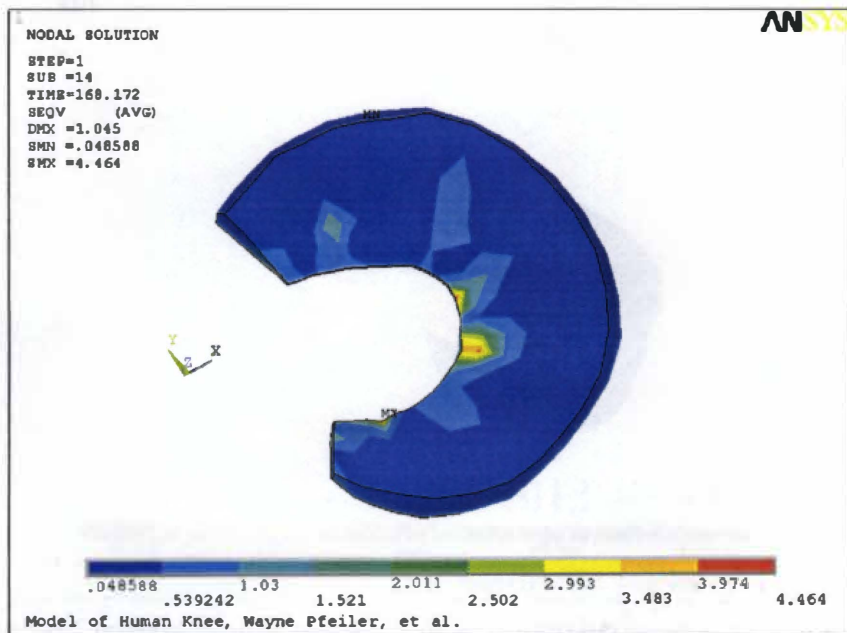


Figure A30: Stress Distribution in Coupled Model Lateral Meniscus

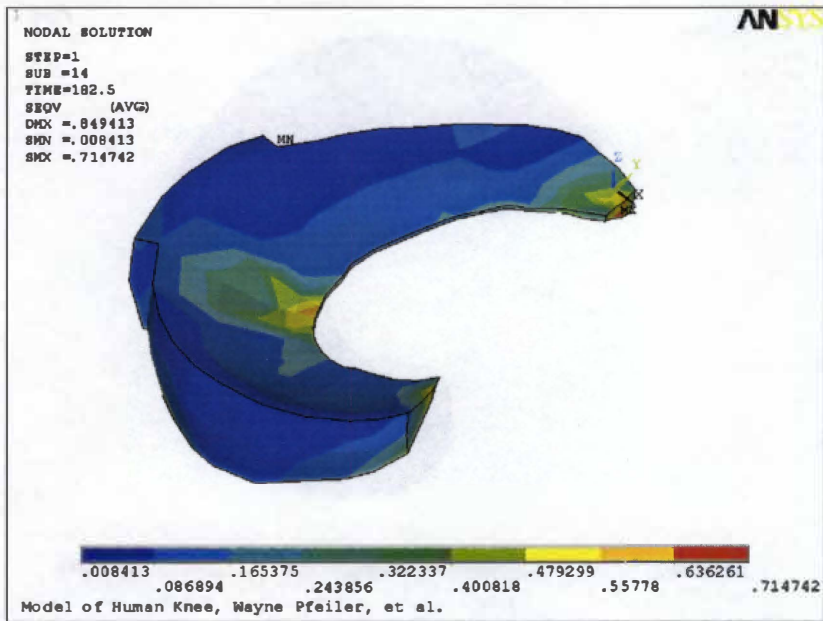


Figure A31: Stress Distribution in Constrained Model Medial Meniscus

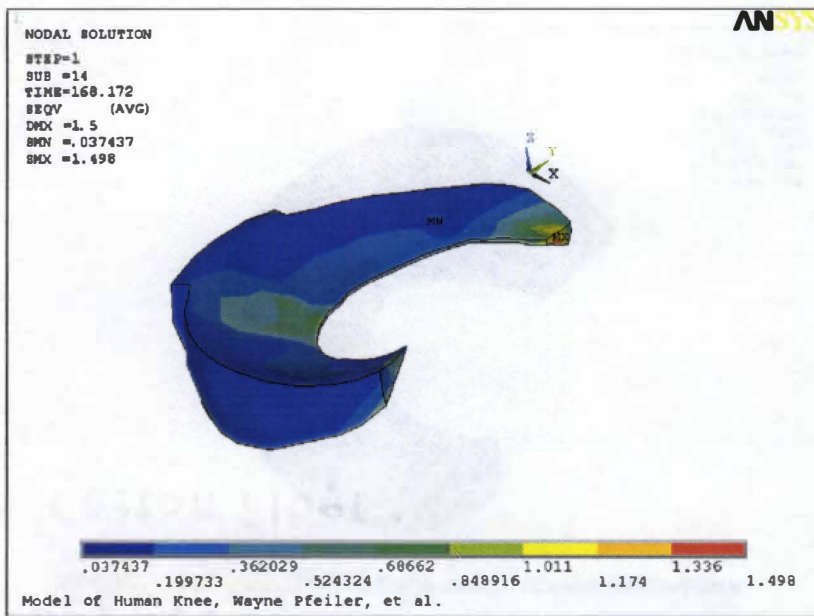


Figure A32: Stress Distribution in Coupled Model Medial Meniscus

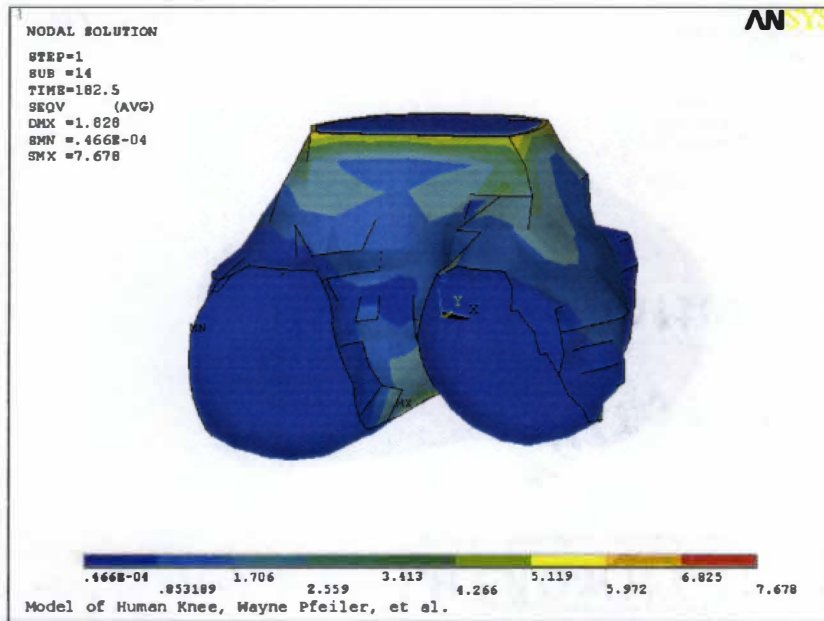


Figure A33: Stress Distribution in Constrained Model Femur

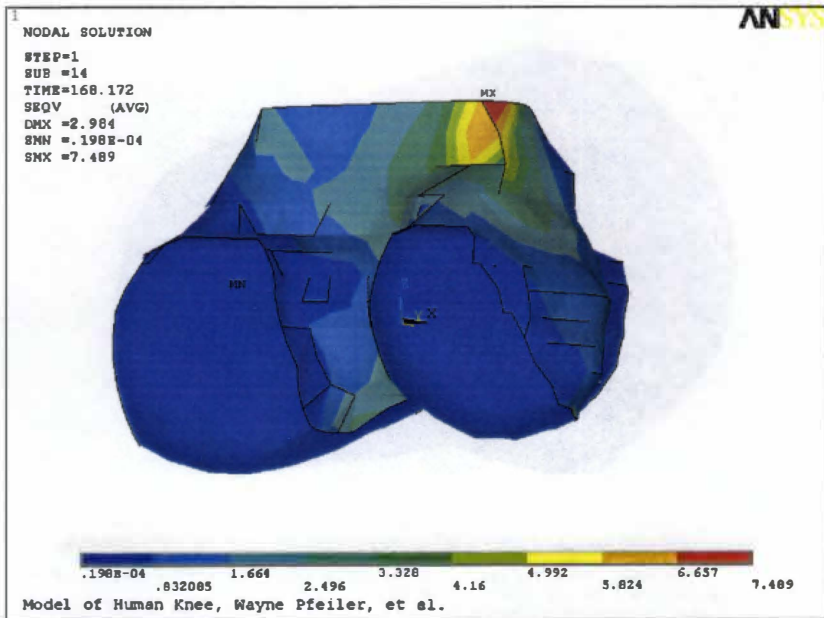


Figure A34: Stress Distribution in Coupled Model Femur

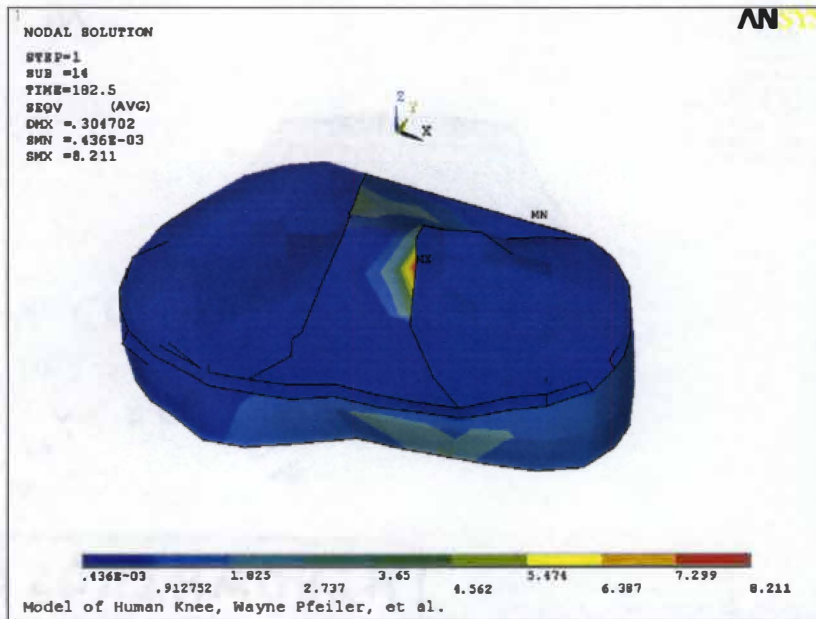


Figure A35: Stress Distribution in Constrained Model Tibia

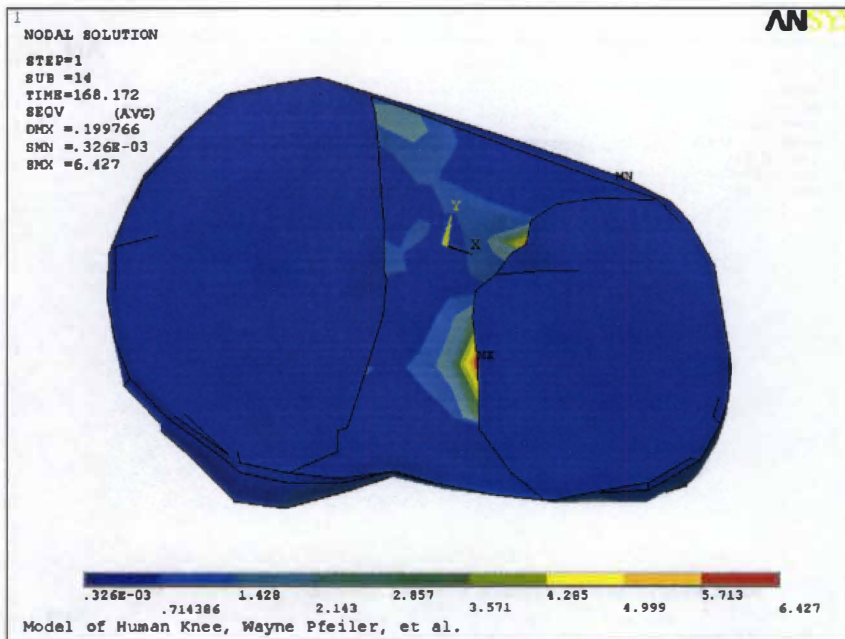


Figure A36: Stress Distribution in Coupled Model Tibia

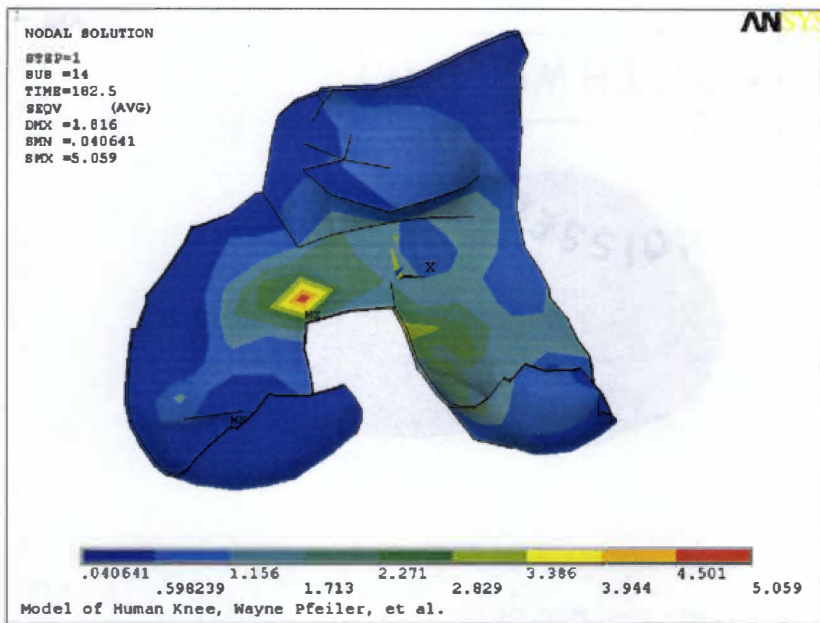


Figure A37: Stress Distribution in Constrained Model Femoral Subchondral Bone

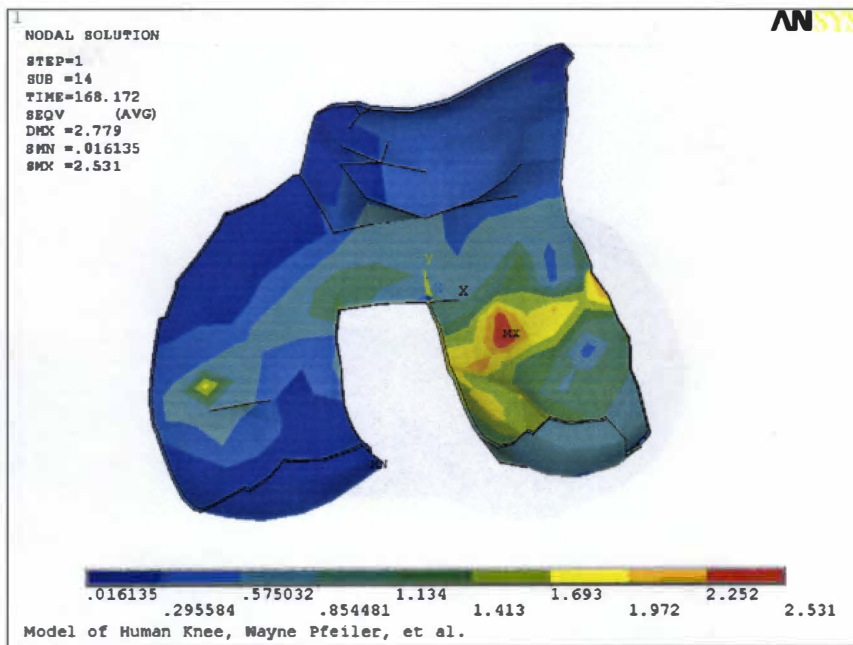


Figure A38: Stress Distribution in Coupled Model Femoral Subchondral Bone

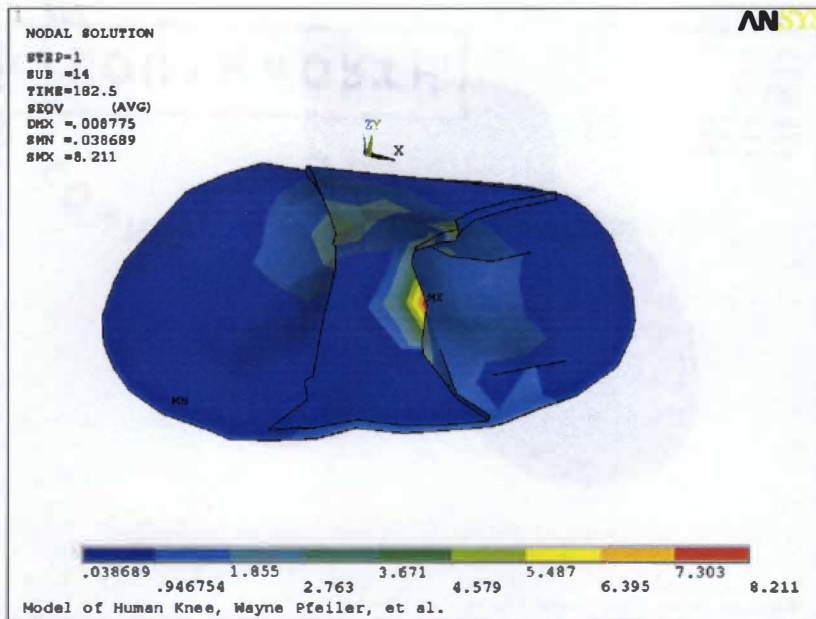


Figure A39: Stress Distribution in Constrained Model Tibial Subchondral Bone

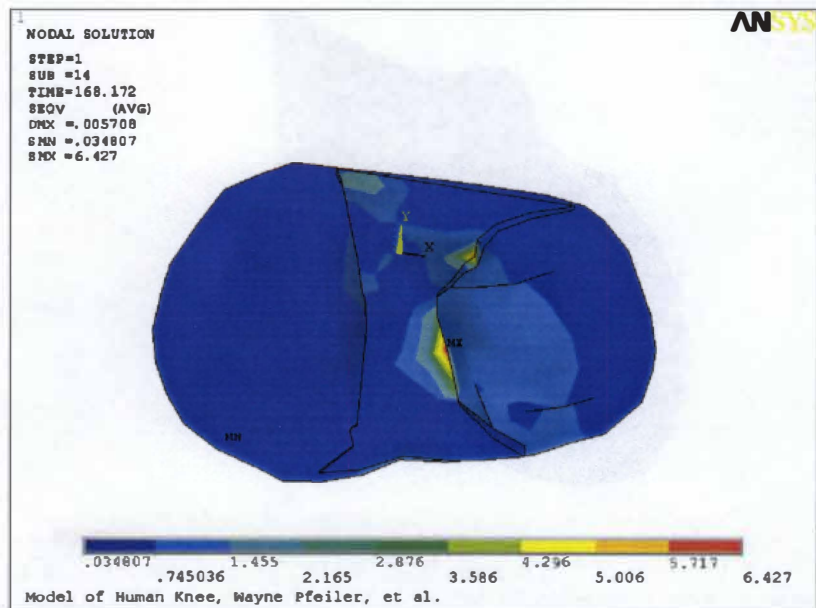


Figure A40: Stress Distribution in Coupled Model Tibial Subchondral Bone

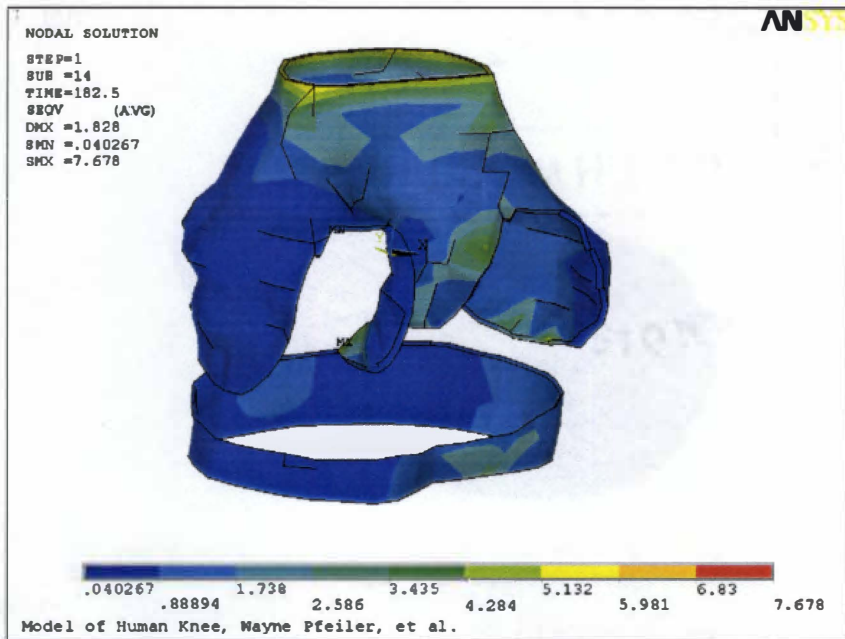


Figure A41: Stress Distribution in Constrained Model Cortical Bone

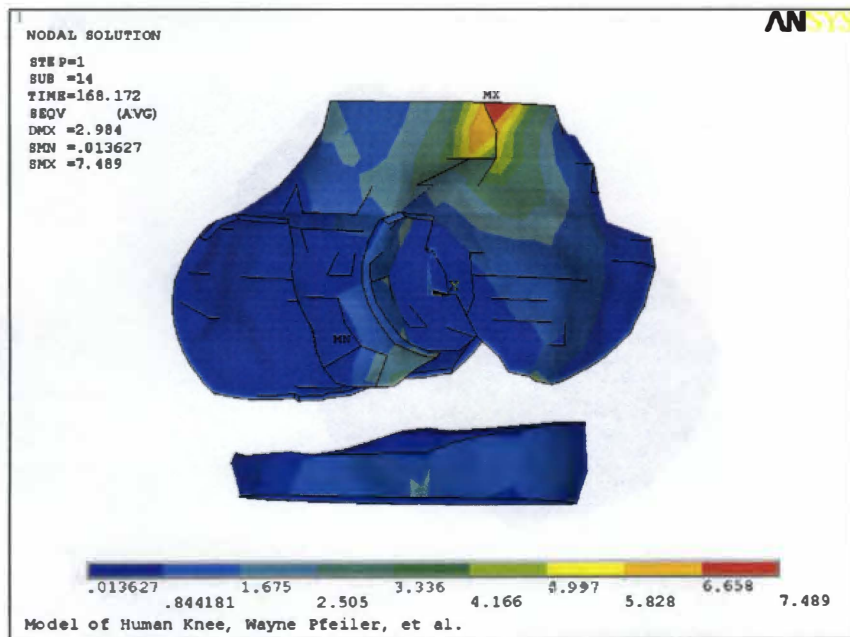


Figure A42: Stress Distribution in Coupled Model Cortical Bone

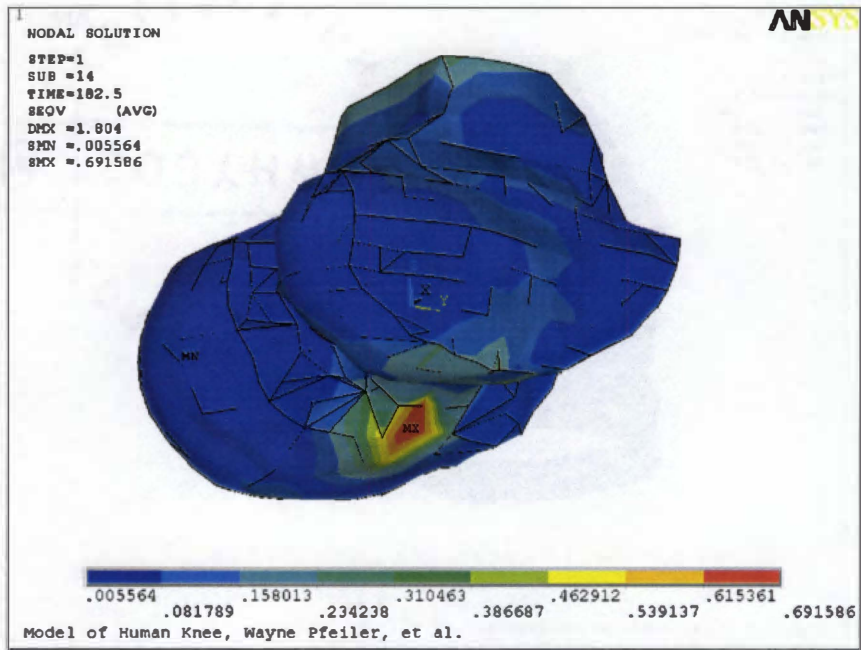


Figure A43: Stress Distribution in Constrained Model Femoral Trabecular Bone

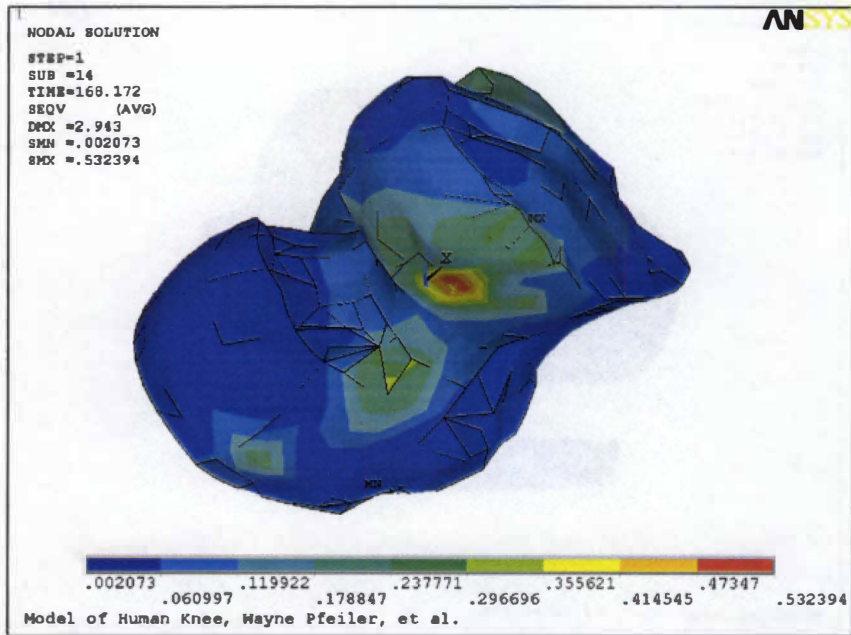


Figure A44: Stress Distribution in Coupled Model Femoral Trabecular Bone

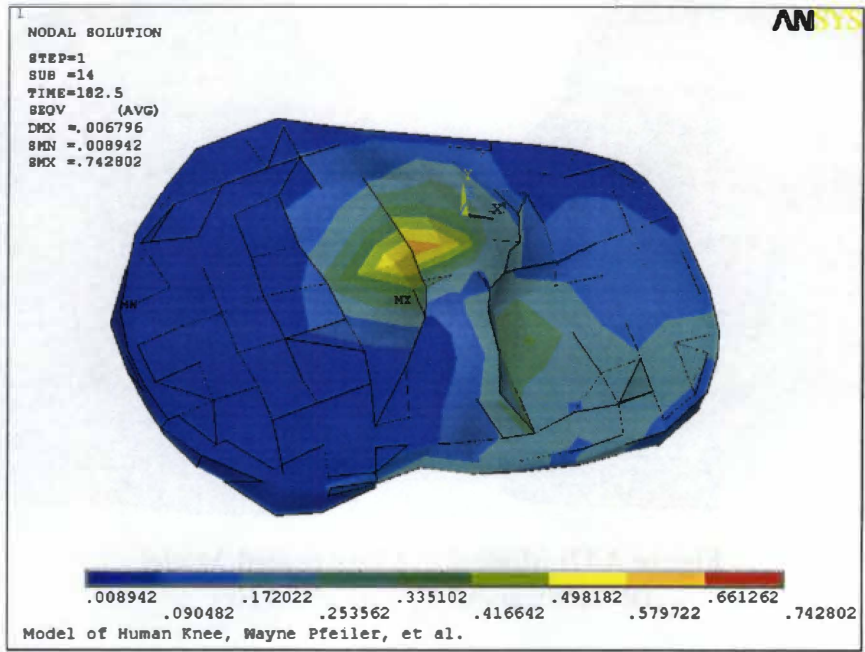


Figure A45: Stress Distribution in Constrained Model Tibial Trabecular Bone

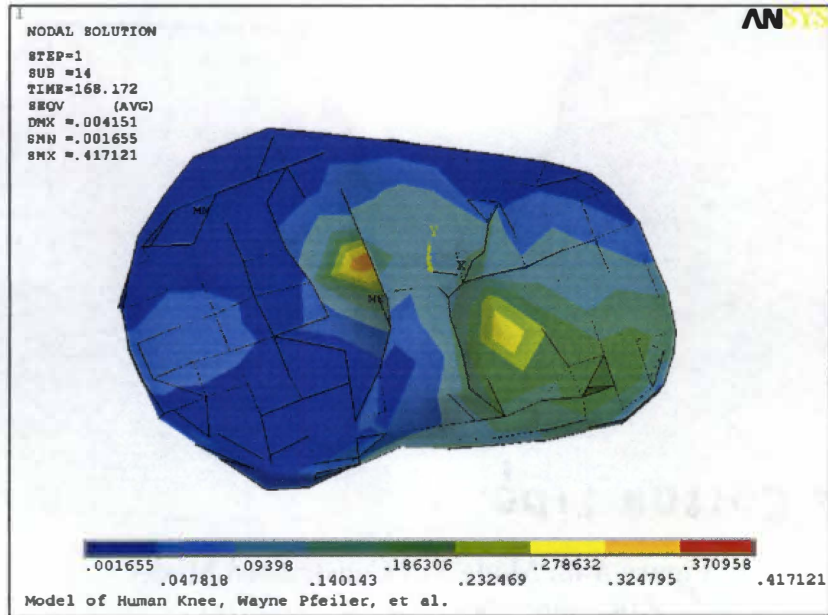


Figure A46: Stress Distribution in Coupled Model Femoral Trabecular Bone

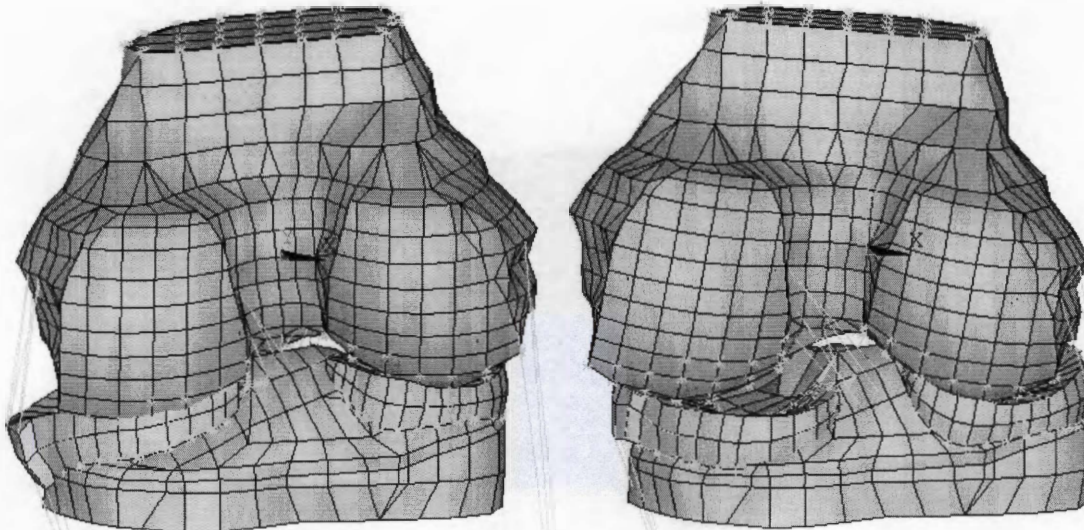


Figure A47: Mode 2 of Constrained Model
(Rotation about Y-axis, 35.78 Hz)

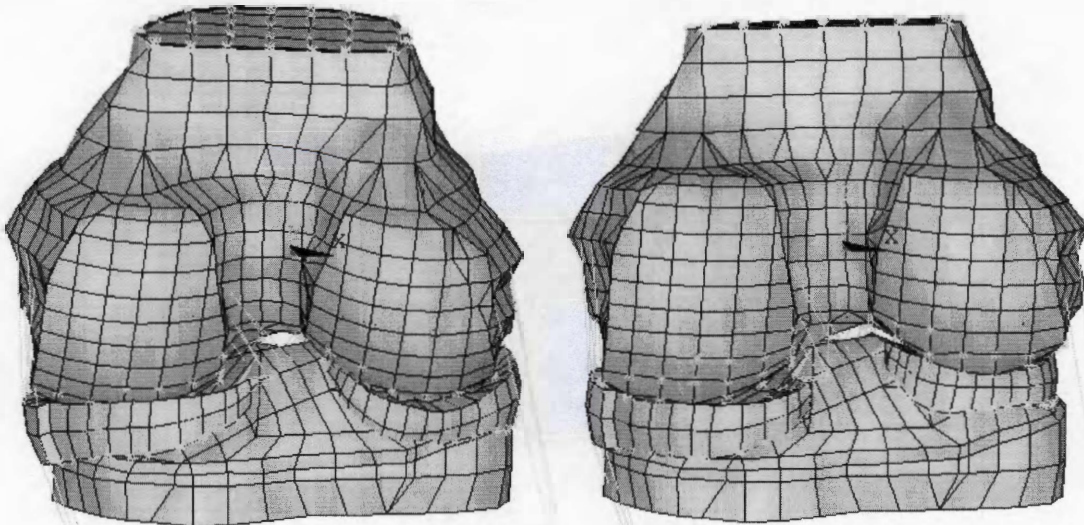


Figure A48: Mode 3 of Constrained Model
(Rotation about X-axis, 79.64 Hz)

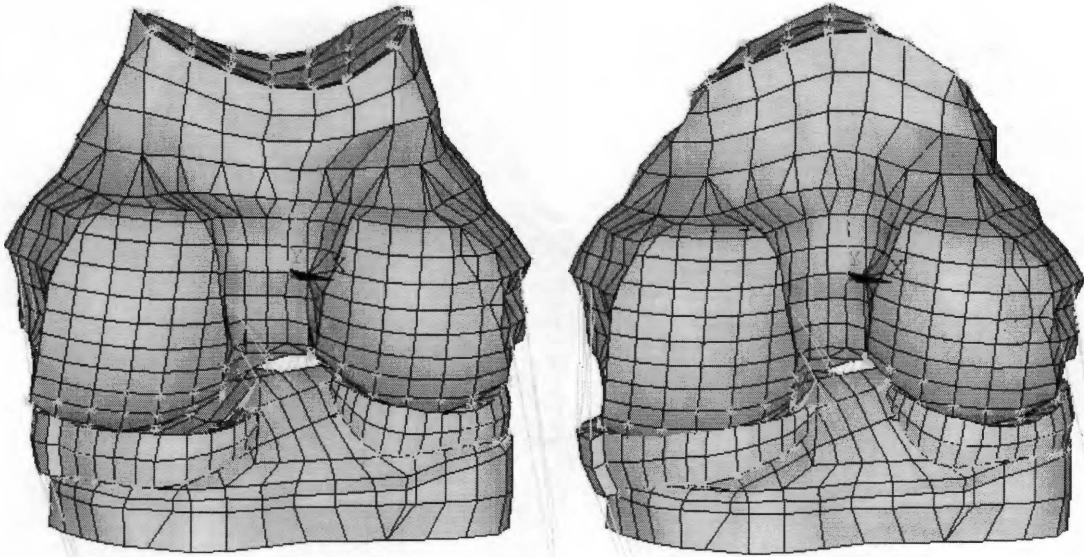


Figure A49: Mode 4 of Constrained Model
(Shaft warping, 240.12 Hz)

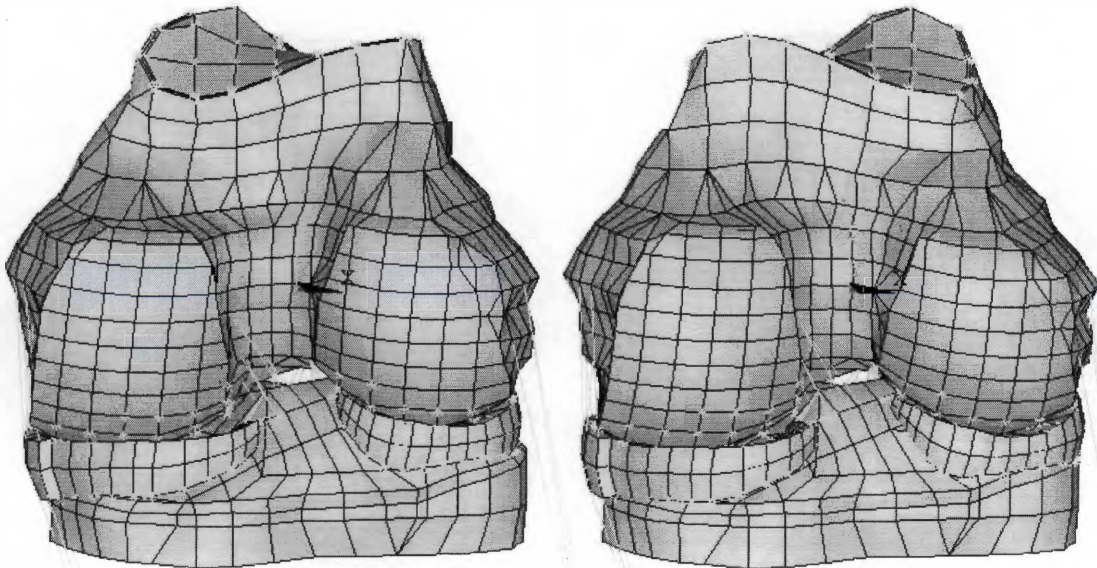


Figure A50: Mode 5 of Constrained Model
(Shaft warping, 244.30 Hz)

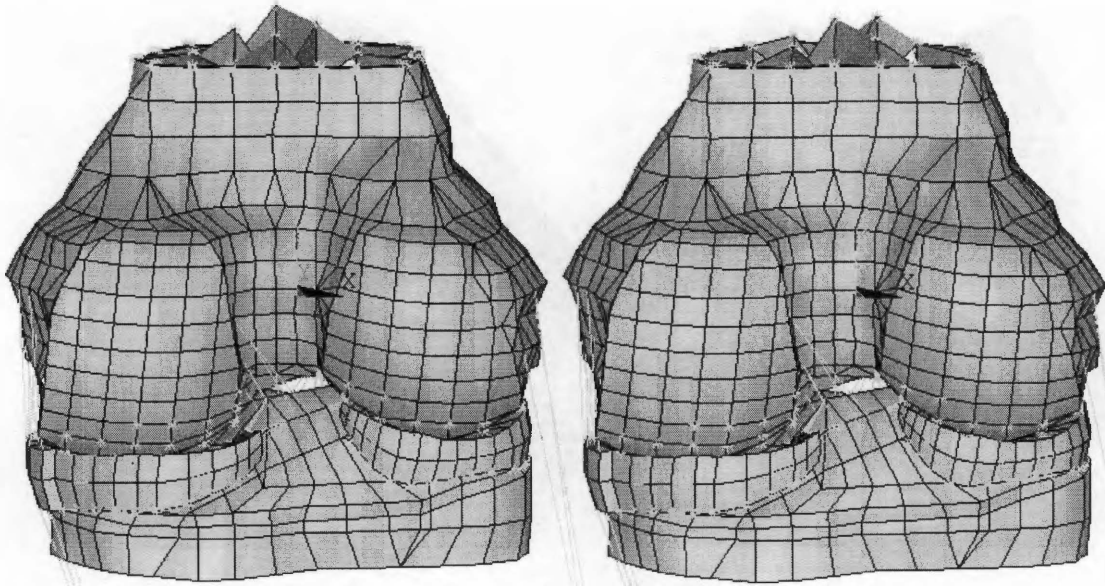


Figure A51: Mode 6 of Constrained Model
(Trabecular oscillation, 261.58 Hz)

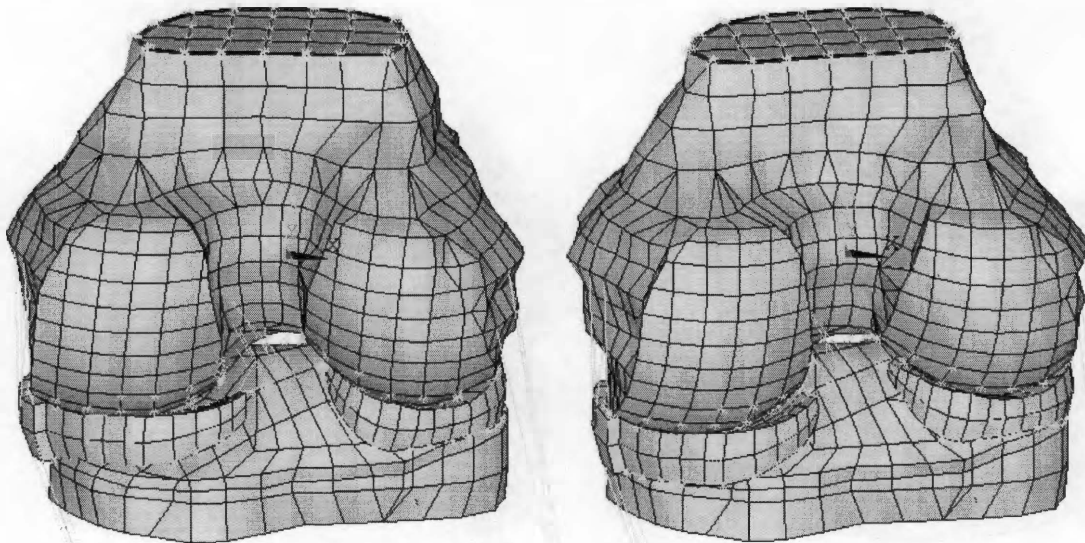


Figure A52: Mode 1 of Coupled Model
(Torsion about Z-axis, 2.55 Hz)

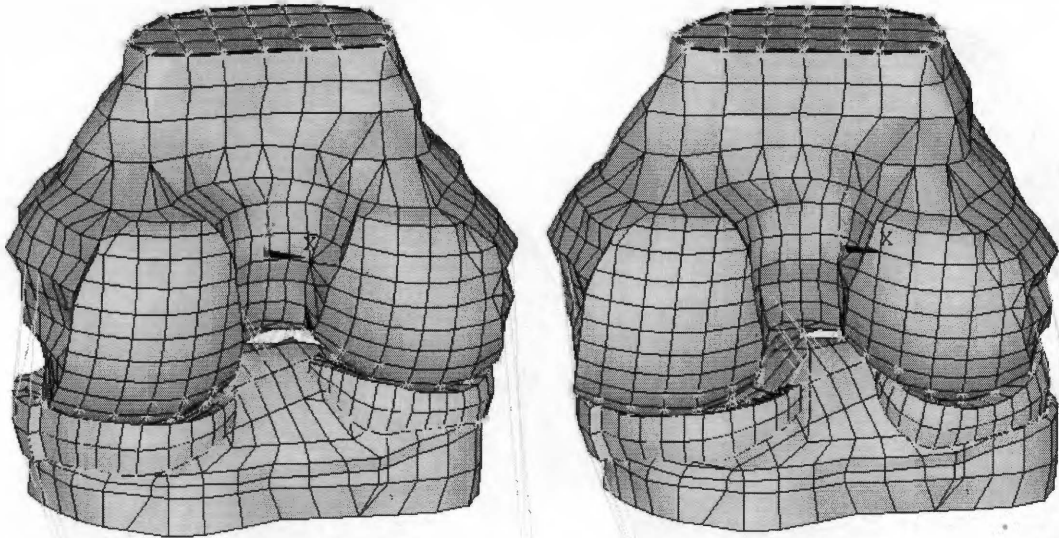


Figure A53: Mode 2 of Coupled Model
(Torsion about Z-axis, 5.98 Hz)

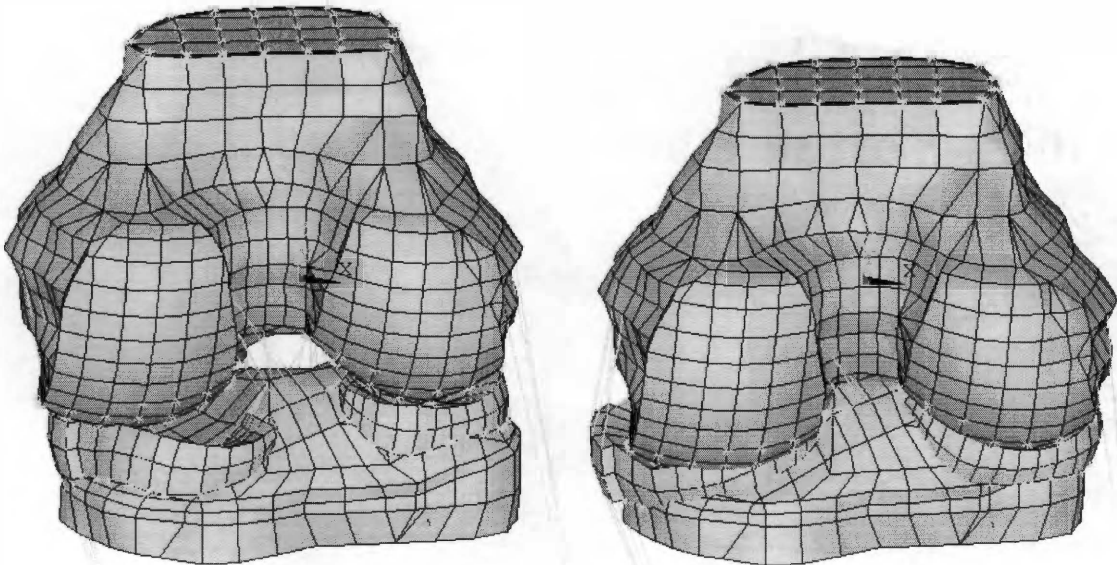


Figure A54: Mode 3 of Coupled Model
(Axial compression, translation, 7.76 Hz)

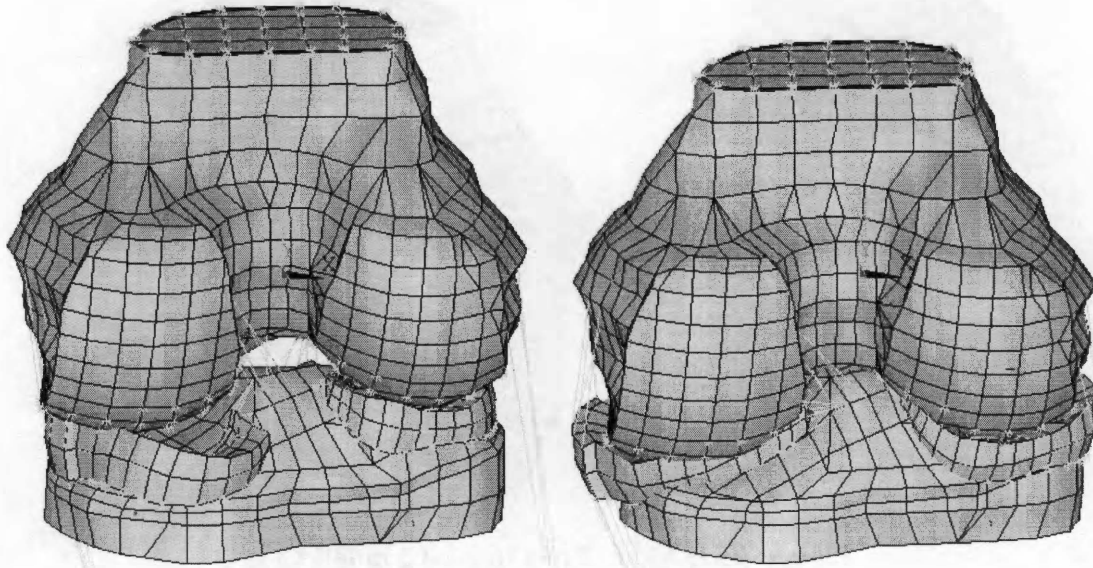


Figure A55: Mode 4 of Coupled Model
(Axial compression, 17.70 Hz)

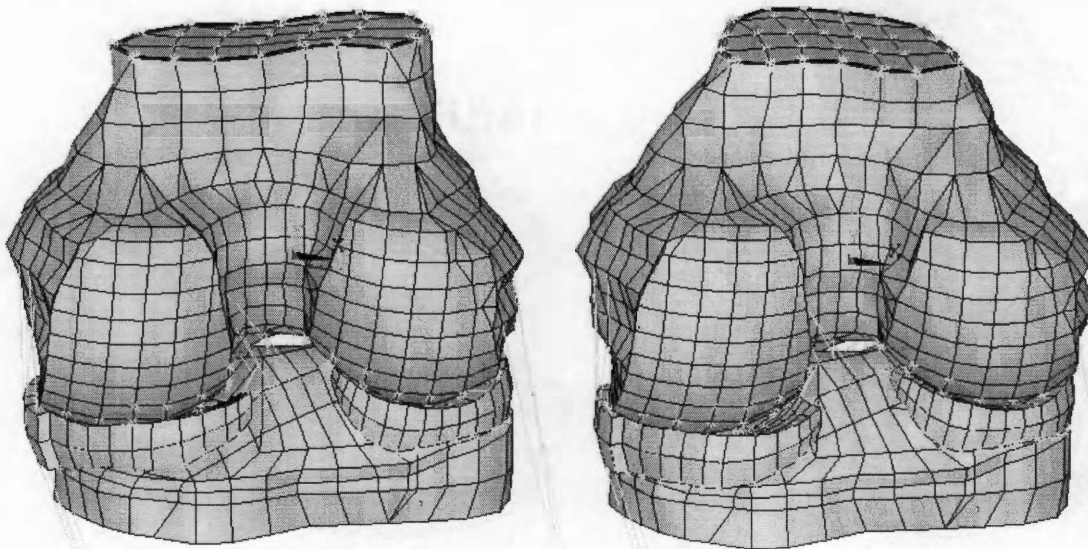


Figure A56: Mode 5 of Coupled Model
(Warping, 126.26 Hz)

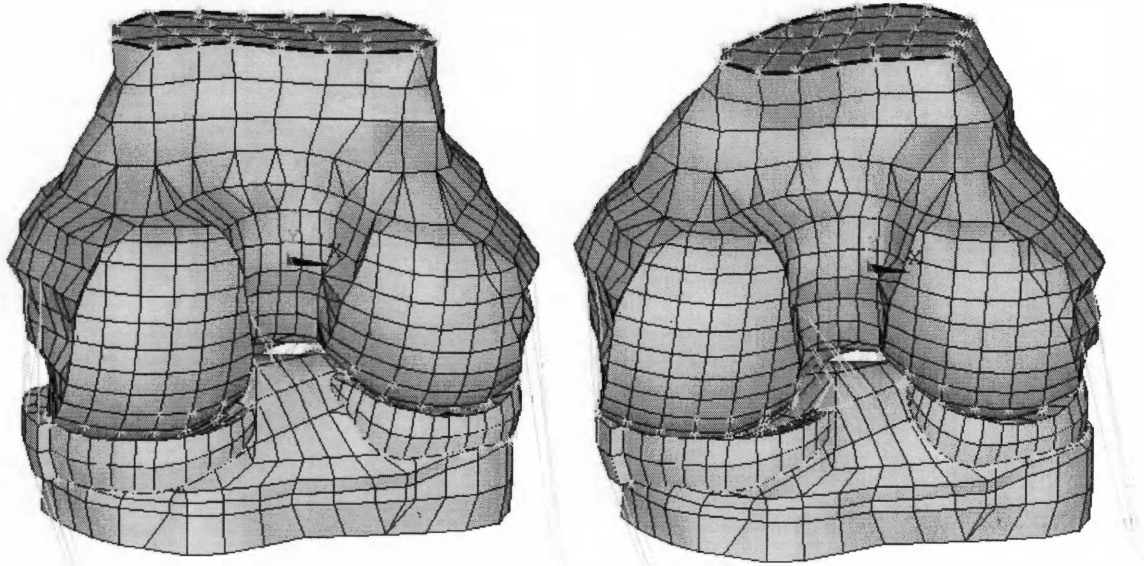


Figure A57: Mode 6 of Coupled Model
(Warping, 127.73 Hz)

Vita

Terry Wayne Pfeiler, Jr. was born in Powell, TN on December 10, 1979. Following a grade school move to Chattanooga, he graduated from Hixson High school in 1998. Next, Wayne continued on to the University of Tennessee at Knoxville where he received a B.S. degree in May 2002 and M.S. degree in May 2004. Currently, Wayne is working as a graduate research assistant while pursuing a doctorate in Biomedical Engineering at the University of North Carolina/North Carolina State University joint graduate program.

Faint, illegible text at the top of the page, possibly bleed-through from the reverse side.

SOUTH WORTH

SECTION

100-50-100-115

5989 2949 7
06/23/04 MFB